Influence of Macroscopic Heat Flow Constrictions on the Performance of Fin/Tube Heat Exchangers

R. O. McGill and A. M. Clausing

ACRC TR-64 July 1994

For additional information:

Air Conditioning and Refrigeration Center
University of Illinois
Mechanical & Industrial Engineering Dept.
1206 West Green Street
Urbana, IL 61801

(217) 333-3115

Prepared as part of ACRC Project 19
An Investigation of Refrigerator/Freezer Insulation Systems
A. M. Clausing, Principal Investigator

The Air Conditioning and Refrigeration Center was founded in 1988 with a grant from the estate of Richard W. Kritzer, the founder of Peerless of America Inc. A State of Illinois Technology Challenge Grant helped build the laboratory facilities. The ACRC receives continuing support from the Richard W. Kritzer Endowment and the National Science Foundation. The following organizations have also become sponsors of the Center.

Acustar Division of Chrysler
Allied-Signal, Inc.
Amana Refrigeration, Inc.
Brazeway, Inc.
Carrier Corporation
Caterpillar, Inc.
E. I. du Pont de Nemours & Co.
Electric Power Research Institute
Ford Motor Company
Frigidaire Company
General Electric Company
Harrison Division of GM
ICI Americas, Inc.
Modine Manufacturing Co.
Peerless of America, Inc.
Environmental Protection Agency
U. S. Army CERL
Whirlpool Corporation

For additional information:

Air Conditioning & Refrigeration Center
Mechanical & Industrial Engineering Dept.
University of Illinois
1206 West Green Street
Urbana IL 61801

217 333 3115

ABSTRACT

The Influence of Macroscopic Heat Flow Constrictions on the Performance of Fin/tube Heat Exchangers

Robert O. McGill

An investigation of the influences of macroscopic constrictions on the thermal performance of plate-fin heat exchangers is described in this report. Parametric studies cover parameter ranges that are typical of the evaporators used in household refrigerators. Exhaustive numerical investigations are presented that show the influences of: (i) the macroscopic contact geometry—the contact between the plate fin and the tube, (ii) the fin parameter—a dimensionless group that governs the fin efficiency, (iii) the fin geometry, (iv) the interstitial conductance, (v) the constriction alleviation caused by the shunting of a part of the heat flow through the frost buildup around the base of the fin, and (v) the effect of fins with collars—an enlarged apparent contact area at the fin/tube interface. Dimensionless parameters and the physical significance of these parameters are deduced that govern the thermal performance of fins with and without constrictions in the heat flow path.

TABLE OF CONTENTS

LIST OF TABLES

LIST OF FIGURES

NOMENCLATURE

a	Macroscopic contact length along interface, m
A	Area, m^2
b	Apparent contact length, m
g	Gap thickness, m
h	Heat transfer coefficient, W/m^2-K
H	Interstitial Conductance, dimensionless
k	Thermal Conductivity, W/m-K
L	Length, m
m	Fin parameter, dimensionless
P	Fin perimeter, m
q	Actual heat flow rate from fin, W
q_{max}	Heat flow rate from an isothermal fin, W
r	Radius, m
R	Resistance, K/W
T	Temperature, K
U	Overall Heat Transfer Coefficient, W/m^2-K
W	Fin width, m

Greek Symbols

δ	One-half fin thickness, m
ϕ	Azimuthal angle, radians
η	Fin efficiency
ω	Relaxation parameter

Subscripts

al	Fin material
b	Base condition
c	Fin collar
cond	Conductive path
conv	Convective path
e	Equivalent fin
f	Fin height
fl	Interstitial fluid
g	Gap condition
g1	Gap condition, annular geometry
g2	Gap condition, rectangular geometry
i, j	Spatial indices
l	Characteristic Length
p	Perfect contact condition
r	Radial direction, rectangular geometry
s	Surface condition
t	Tip condition
∞	Ambient condition

Superscripts

*	Dimensionless quantity

1. INTRODUCTION

1.1 Objectives

The four primary objectives of this investigation are the following. First, review all relevant literature in order to examine the validity of previously made assumptions and testing methods to the title problem. Secondly, present the results of an exhaustive numerical investigation of the influence of macroscopic heat flow constrictions on fin efficiency for a variety of fin geometries. Thirdly, determine the influence of the fluid or frost filled interstices and the constriction alleviation caused by the shunting of a part of the heat flow through frost buildup surrounding the base of the fin. Fourthly, examine the effects of fins with collars or with an enlarged apparent contact area at the fin/tube interface.

1.2 Background

Many fin/tube heat exchangers have their primary heat transfer surface, the exterior of the tubes, and their secondary surface, the fins, bonded mechanically rather than welded, brazed or soldered (metallurgical bonds). Some examples of these heat exchangers, also known as extended surface or plate-fin heat exchangers, are many of the evaporators used in refrigerators and air conditioning systems, along with "radiators" used in hot water heating systems. There are several manufacturing techniques used to mechanically bond the aluminum fins to the copper tubes, the most common combination. One of these techniques involves using hydraulic pressure or an expansion tool, called a bullet, to radially expand the tube, in the tube holes of the fins, past contact with the fin stock, see Figure 1.1. The fins are commonly provided with formed collars which provide a greater area of contact with the tube and a means of uniformly spacing the fins. Another technique involves deforming the tubes after they are placed into the slotted fin stock, see Figure 1.2. No matter what technique is employed, imperfect contact at the fin/tube interface, microscopic and macroscopic, is always present. This imperfect contact creates two paths of heat flow at the interface: conduction through the metal-to-metal contact points and conduction through the fluid occupying the interstices. Note that the radiative heat transfer across the gap is almost always negligible in this application.

The macroscopic constriction to heat flow in the fins, the so-called thermal constriction resistance, is often the dominant resistance in the air-side heat flow path and is related to the total resistance at the joint by the following equation:

$$R_c = R_t - R_p \tag{1.1}$$

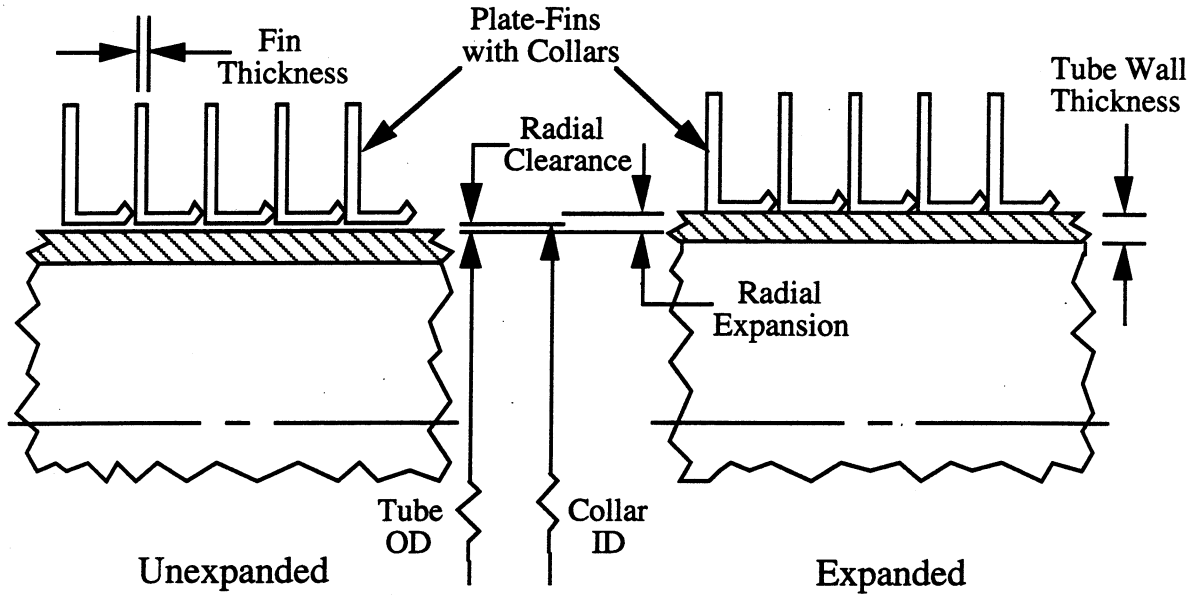

Figure 1.1. Axial Cross Section of Collared Fins and Tubes Before and After Expansion

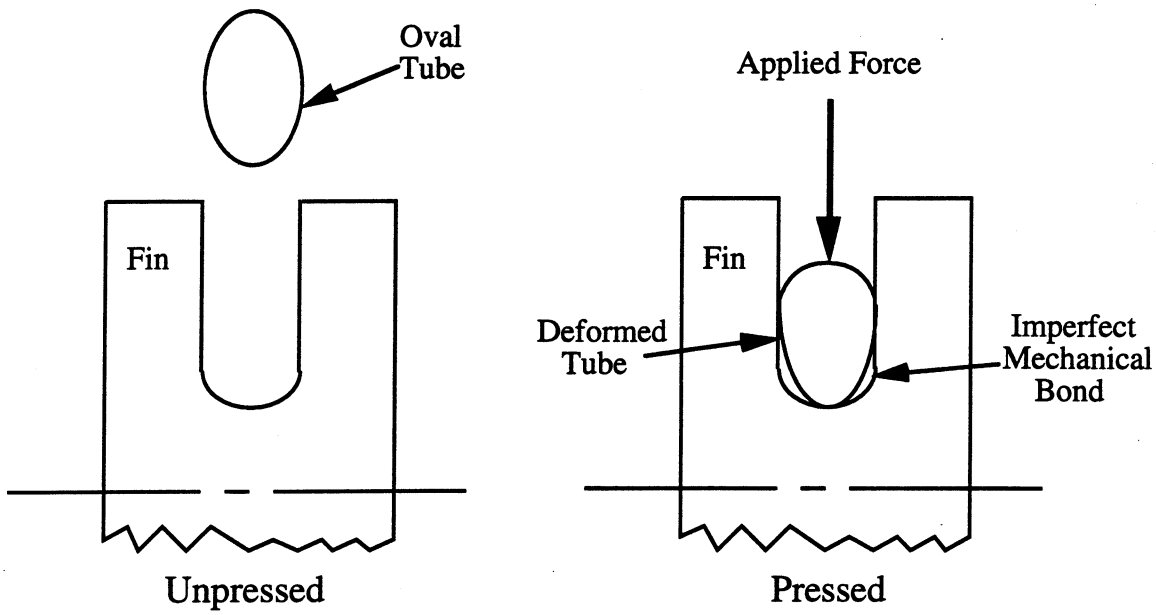

Figure 1.2. Mechanical Bond Created by Tube Deformation

where R_c is the thermal constriction resistance, R_t is the total resistance across the entire heat flow path and R_p is the resistance to heat flow with perfect contact at the joint. The total resistance of the heat flow path across the joint is defined:

$$R_t = \frac{\Delta T}{q} \tag{1.2}$$

where ΔT is the driving potential divided by the heat flow rate, q. When dealing with microscopic constrictions, where a uniform boundary condition is commonly assumed at the fin/tube interface, this constriction resistance is ordinarily referred to as the thermal contact resistance. The inverse of the thermal contact resistance is known as the contact conductance.

2. LITERATURE SURVEY

2.1 Previous Studies - Contact Resistance

Extensive research of thermal contact resistance has been completed for many different applications. Madhusudana and Fletcher (1986), Yovanovich (1986) and Fletcher (1988) provide excellent summaries of recent developments. Past studies of contact resistance in finned-tubes has been summarized by Hrnjak and Sheffield (1990) and will be expanded upon below. All previous investigators of fin/tube heat exchangers have assumed that the interface surface was macroscopically conforming. This assumption is unrealistic, for most cases, and the magnitude of macroscopic constrictions must be determined. Although the study of macroscopic constrictions is not new (see for example: Clausing, 1963 and 1965; Tio and Sadhal, 1991 and 1992), the application to fin/tube heat exchangers has been ignored. In addition, all previous experiments of fin/tube geometries have taken place in a vacuum environment, or the plate-fins have been insulated in such a way as to eliminate convective heat loss. Thus, correlations developed from these experimental data have no justifiable application to plate-fin heat exchanger designs.

The first attempt to determine the influence of the fin bond on heat transfer was made by Dart (1959). Dart designed an experimental method which is still widely used today with some modifications. His method involved passing hot and cold water through adjacent tubes of a tube bank, connected by collared fins, and taking temperature measurements before and after each pass. By knowing the thermal conductivity of the tubes and fins, the temperature difference of the water, the mass flow rate of the water and eliminating convective heat transfer, by insulating the apparatus, the additional resistance in the *conductive path* could be determined. Dart concluded that this conductive resistance at the fin/tube interface is significant when compared with the overall conductive resistance.

Gardner and Carnavous (1960) studied the gap resistance of axially, helically and circularly finned-tubes which were mechanically embedded, metallurgically bonded, interference fitted or tension wound. Gardner and Carnavous predicted the thermal contact resistance, of the tube banks, in terms of contact pressure, thermoelastic expansion, operating temperature and fin dimensions. Fairly good agreement was achieved between their analytical theory and experimental results. Their conclusions were again verified by Young and Briggs (1965). Gardner and Carnavous concluded that thermal contact resistance only became significant at elevated operating temperatures where differential thermal expansion between the fin and the tube caused a complete loss of contact pressure; Taborek (1987) specifically established these elevated temperature limits for various fin geometries and materials. Application of their results to fin/tube heat exchangers can not easily be

made because the assumption of a concentric gap at the interface is made and the fin/tube bonds studied are not similar.

Eckels (1977) expanded upon the research performed by Dart. He developed a semi-theoretical correlation to predict the effect of varying fin number (fins per meter), fin thickness and tube diameter on thermal contact resistance for mechanically expanded, fin/tube heat exchangers. His experimental apparatus was almost identical to Dart's, hot and cold water was circulated through adjacent tube rows so that heat flow through the tube walls, fin collars and fins would occur. Eckels made much more precise temperature and mass flow rate measurements than Dart; hence, his results are more accurate. In addition, Eckels used electrically conducting paper models of the fin to verify the conductive resistance of the fin. Like Dart, convective effects were minimized by insulating the tested coils; hence, a conduction problem was studied. Eckels concluded that the contribution of thermal contact resistance to the overall conductive resistance ranged from being insignificant to 15% for the mechanically expanded, fin/tube heat exchangers tested.

Christensen and Fernandes (1983) studied the thermal and fouling resistances of pneumatically expanded tubes of a fin/tube heat exchanger. Unfortunately, their calculated resistance values fell within the domain of their error analysis. The authors concluded that their experimental study had been successful in estimating the order of magnitude of contact and fouling resistances.

During the past decade, most of the research on thermal contact resistance of fin/tube heat exchangers has been performed at the University of Missouri-Rolla under Sheffield and Sauer. Preliminary investigations of the mechanical fin/tube bond and of surface characteristics of a fin/tube heat exchanger to predict contact geometry were performed by Ernest et al. (1985) and Sheffield et al. (1985) respectfully. The first empirical correlation of thermal contact conductance for eight mechanically expanded fin/tube heat exchangers, 9.53 mm (0.375 inch) tubes, of differing geometries (fins per meter, fin thickness and net interference) was developed by Sheffield et al. (1985). A variation of Dart's experimental method was employed. The two most significant changes to the method were: (i) a three row fin/tube heat exchanger was used where hot water was circulated through the center row and cold water through the top and bottom rows, and (ii) all heat exchanger evaluations were conducted in a vacuum environment. Thus, the thermal contact conductance could simply be calculated from experimental data for each heat exchanger tested (along with defined parameters), and a correlation developed in terms of fin number, fin thickness, unexpanded tube diameter and net interference. Note that net interference (I) is defined as:

$$I = \frac{(d_e + 2\delta - d_n)}{2} \tag{2.1}$$

where d_e is the expansion tool diameter, δ is the tube wall thickness and d_n is the inside diameter of the fin collar. Detailed bar graphs of the results can be found in Sauer and Sheffield (1987). For the heat exchangers with 787 fins per meter (20 fins per inch), 551 fins per meter (14 fins per inch) and 236 fins per meter (6 fins per inch) with varying net interferences, the thermal contact resistance accounted for 5 to 12%, 11 to 19% and 6 to 8% of the overall conductive resistance to heat flow, respectfully. Note that the heat exchangers with 236 fins per meter had a lower thermal contact resistance due to the longer collar on these fins, thus a larger contact area with the tube.

Sheffield et al. (1987, 1989) continued their previous research in an attempt to generalize their correlation for fin/tube heat exchangers to include various tube diameters. The experimental apparatus and conditions were identical to the previous investigation. The newly developed correlation was now restricted to radially expanded, fin/tube heat exchangers with varied tube diameters of 6.35 to 15.9 mm (0.25 to 0.625 inch), fin densities of 236 to 709 fins per meter (6 to 18 fins per inch), fin thicknesses of 0.11 to 0.23 mm (0.0045 to 0.0091 inch) and net interferences of 0.08 to 0.19 mm (0.003 to 0.0075 inch). Of the 31 coils tested, 15 had a measured thermal contact conductance within ± 20% of the predicted conductance. Eleven coils were under predicted by greater than 20% and 5 coils were over predicted by greater than 20%. The thermal contact resistance was determined to range from 5 to 16% of the overall conductive resistance.

Similar research has been performed at the University of Waterloo in Ontario, Canada by Yovanovich et al. Lemczyk and Yovanovich (1987) discussed new models for predicting thermal contact resistance and their application to fin/tube heat exchangers. Their analytical results showed an increase in thermal contact resistance as the initial contact pressure at the fin/tube interface was decreased. In addition, joint resistance increased as the surface roughness increased.

Nho and Yovanovich (1989) performed a similar study as Sheffield et al. (1987). Their test cores were in counter flow where hot water passed through the center tube of the core while cold water passed through six surrounding tubes. Once again, all experimental measurements took place in a vacuum environment. Five test cores were examined with the only two variables of the experiment being fin collar length and expansion tool size. The thermal contact resistance ranged from 18 to 32% of the overall resistance to heat flow.

2.2 Previous Studies - Frost Effects

The accumulation of frost on heat exchanger surfaces has been a major obstacle in improving the performance of refrigeration systems. Frost buildup occurs when moist air passes over heat exchanger coils operating below freezing. Two major detrimental effects result: (i) frost tends to insulate the heat exchanger surface, thus lowering the heat transfer rate and (ii) airflow area across the heat exchanger is reduced, thus an increased pressure drop, and a reduced airflow rate, is experienced across the coil. These detrimental effects of frost buildup on heat exchanger performance have been investigated for many years. Kondepudi and O'Neal (1987) provide a comprehensive literature review of the first 30 years of work. The summary of previous studies discussed here is in no way complete; this survey only highlights previous research which pertain specifically to this investigation, that is, the effect of frost buildup on the heat transfer rate and fin efficiency of fin/tube heat exchangers.

One of the earliest investigations of this phenomenon was by Stoecker (1957). Stoecker studied the behavior of two fin/tube heat exchangers under frosted conditions; one coil having a narrow fin spacing (354 fins per meter, 9 fins per inch) and one having a wide fin spacing (157 fins per meter, 4 fins per inch). Stoecker established an interesting trend in the overall heat transfer coefficient, U, of both heat exchangers; when frost first begins to form on either coil , an increase in U of approximately 5-6% is measured. As the frost layer increases, U eventually decreases due to the insulating effect of the frost. Stoecker attributed this increase in performance to an increase of heat transfer area as a result of increased surface roughness during the onset of frost. Specific trends in fin efficiency were not discussed and the extent of contact at the fin/tube interface was not described.

A variety of fin/tube heat exchanger geometries were tested in conjuction by Gates et al. (1967) and Huffman and Sepsy (1967) under frosted conditions. These tests were performed in a similar manner as Stoecker's experiment. Both papers acknowledge from previous investigations that initial frost buildups are beneficial from a heat transfer point of view; however, they do not draw any conclusions on this point from their experimental results. They do state that initial frost accumulation does not result in a significant pressure drop across the coil. While the papers do not mention any trends in fin efficiency, they do mention that the fin/tube interfaces of the coils tested were brazed as to eliminate contact resistance.

Finally, the most recent and comprehensive study of the problem was performed by Kondepudi and O'Neal (1993). Kondepudi and O'Neal first developed a rigorous simulation model, lacking from previous investigations, and then conducted experiments, again similar to Stoecker's, to

prove their models predicted actual behavior of fin/tube heat exchangers under frosted conditions. Their model did not predict an increase in U at any time during the frost accumulation. They attributed this to airside heat transfer data, frost surface roughness and fan characteristics not being incorporated within the model. The U values obtained from the experimental results fell within 15-20% of the model predictions, but did not show any definite advantage in performance during initial frost formation. Contact resistance at the fin/tube interface was not considered during their model development and the variation of fin efficiency with frost buildup was ignored.

The question now posed is could the slight increase of U during initial frost accumulation, established by Stoecker in 1957 and recognized by most research since, be a result of a decrease in thermal contact resistance rather than an increase of heat transfer area via increased surface roughness? Frost buildup at the fin/tube interface could result in the partial alleviation of any constriction resistance leading to an increase in fin efficiency. The previous studies summarized above suggest this possibility.

2.3 Application to Plate-Fin Heat Exchanger Designs

Although the effect of thermal contact resistance to fin/tube heat exchangers has been studied by many individuals over the past 30 years, attempts to predict this resistance are generally not valid for plate-fin heat exchanger designs because of the following reasons:

(i) All previous investigations have assumed a macroscopically conforming interface.
(ii) Tests performed in a vacuum environment over estimate the actual resistance because of no interstitial fluid.
(iii) All previous investigations have eliminated convective heat loss and forced an adiabatic boundary condition on the fin surfaces; hence, conduction problems were studied whereas extended surfaces are of interest.
(iv) Only fin/tube heat exchangers with formed collars have been studied.
(v) All previous investigations have ignored the possibility of heat flow constriction alleviation at the onset of frost accumulation at the fin/tube interface.

In order to justify each of the reasons (except the logical fourth and fifth restriction), the following simple investigations will prove the significance of macroscopic constrictions, conduction through interstitial fluids and a convective boundary condition over the fin surfaces. Note that the results of these simple investigations are not meant to predict the performance of the plate-fins used in typical fin/tube heat exchangers. Relevant geometries are to be used in the title investigation.

The case of steady heat flow in a straight fin of rectangular profile was analyzed in order to determine the influence of the constriction ratio on the fin efficiency. The geometry investigated is a fin of length L, width 2b and thickness 2δ. Perfect contact was assumed over a portion of the base of width 2a, and the balance of the base area was considered to be adiabatic. A symmetrical section of this fin is illustrated in Figure 2.1.

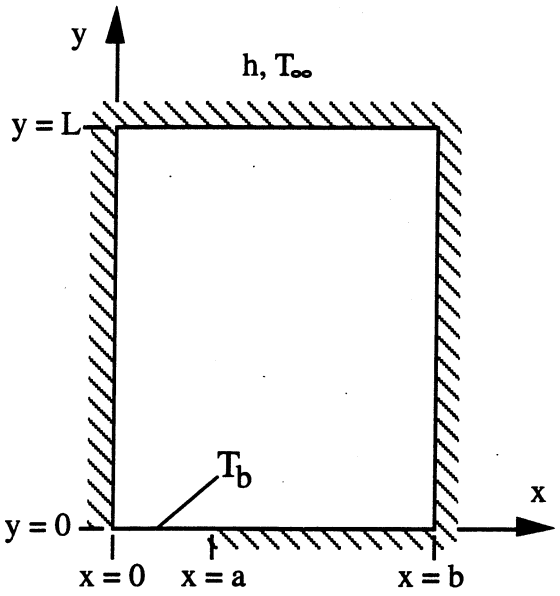

Figure 2.1. Symmetrical Section of Extended Surface Investigated

Because of the mixed boundary condition at the base, y = 0, a numerical, finite-difference solution was effected. The base temperature of the contact area, T_b, the ambient fluid temperature, T_∞, the thermal conductivity of the fin, k, and the convective heat transfer coefficient, h, were assumed to be specified constants. The heat exchanged between the fin and the surrounding fluid, q, was calculated from the discrete temperatures determined in the finite-difference solution. The actual heat exchanged by the fin is then divided by the theoretical maximum possible heat flow rate from the fin, q_{max}, in order to calculate the fin efficiency, η. The maximum possible heat flow rate is the heat flow from the fin that would occur if the entire fin area were at the base temperature, that is:

$$q_{max} = 2bLh\left(T_b - T_\infty\right) \tag{2.2}$$

and

$$\eta = \frac{q}{q_{max}} \tag{2.3}$$

The variation of the fin efficiency with the constriction ratio is illustrated in Figure 2.2 for various values of b/L. A value of the fin parameter, m, of 1.419 (optimum fin) was used for the cases presented in Figure 2.2 where m is defined as:

$$m \equiv \left[\frac{h L^2}{k \delta}\right]^{1/2} \tag{2.4}$$

Note that m^2 is a ratio of the conductive resistance of the fin, $\frac{L}{k (\delta W)}$, to the convective resistance between the fin and the fluid, $\frac{1}{h (WL)}$. The strong influence of the contact area on the fin efficiency is clearly shown in this figure. Seemingly, to disagree with the conclusions made by Manzoor et al. (1984).

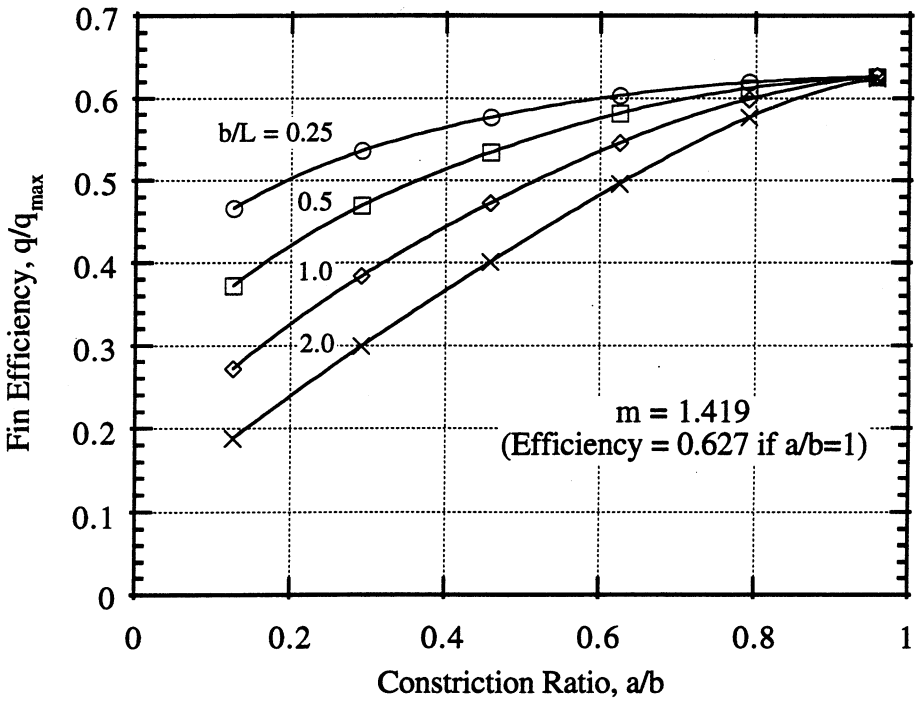

Figure 2.2. Influence of Constriction Ratio on Fin Efficiency for Various Values of b/L

By changing the boundary condition at the base, y = 0, in the above investigation, the effect of an interstitial fluid in the gap may be determined. Once again, perfect contact was assumed over a portion of the base width 2a; while, the balance of the base area was assumed to have conductive heat flow across a constant and specified air gap. Figure 2.3 illustrates the effect of various gap thicknesses on the fin efficiency keeping the other parameters from the first investigation constant. The strong influence of the air gap thickness (or conductance) on the fin efficiency is shown in the figure.

Finally, a brief comparison of the constriction resistance between a pure conduction problem similar to previous studies and the comparable extended surface problem that should have been considered, see Figure 2.4, is presented. As defined, the constriction resistance is:

$$R_c = R_t - R_p \tag{2.5}$$

where R_t is the total resistance across the interface and R_p is the resistance to heat flow with perfect contact at the joint. When this constriction resistance is nondimensionalized by R_p, a suitable parameter now exists to compare the problems. For the conduction problem, the dimensionless

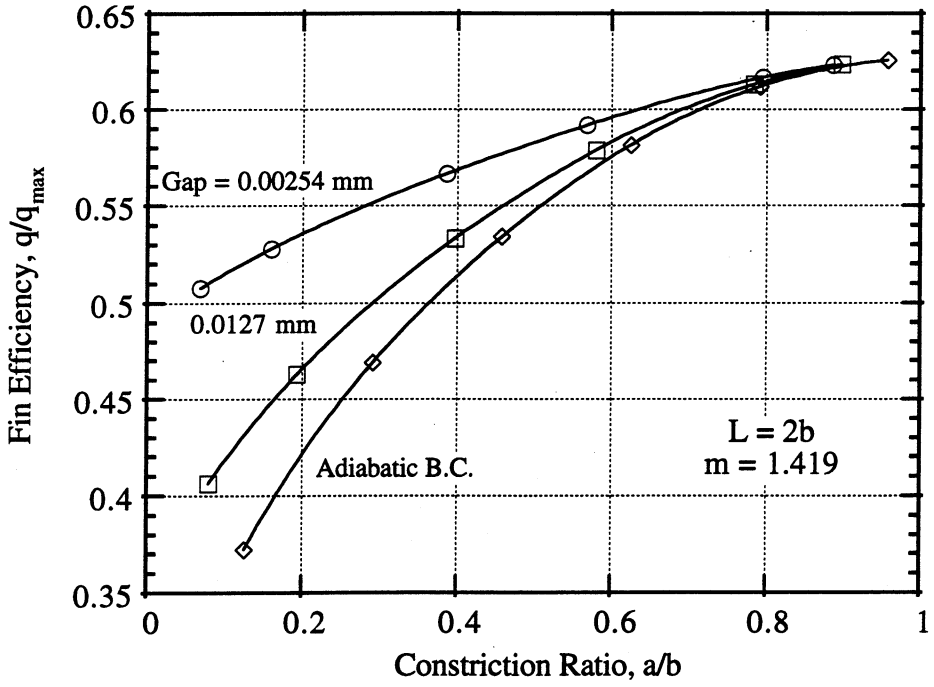

Figure 2.3. Effect of Conduction Through Interstitial Air on Fin Efficiency

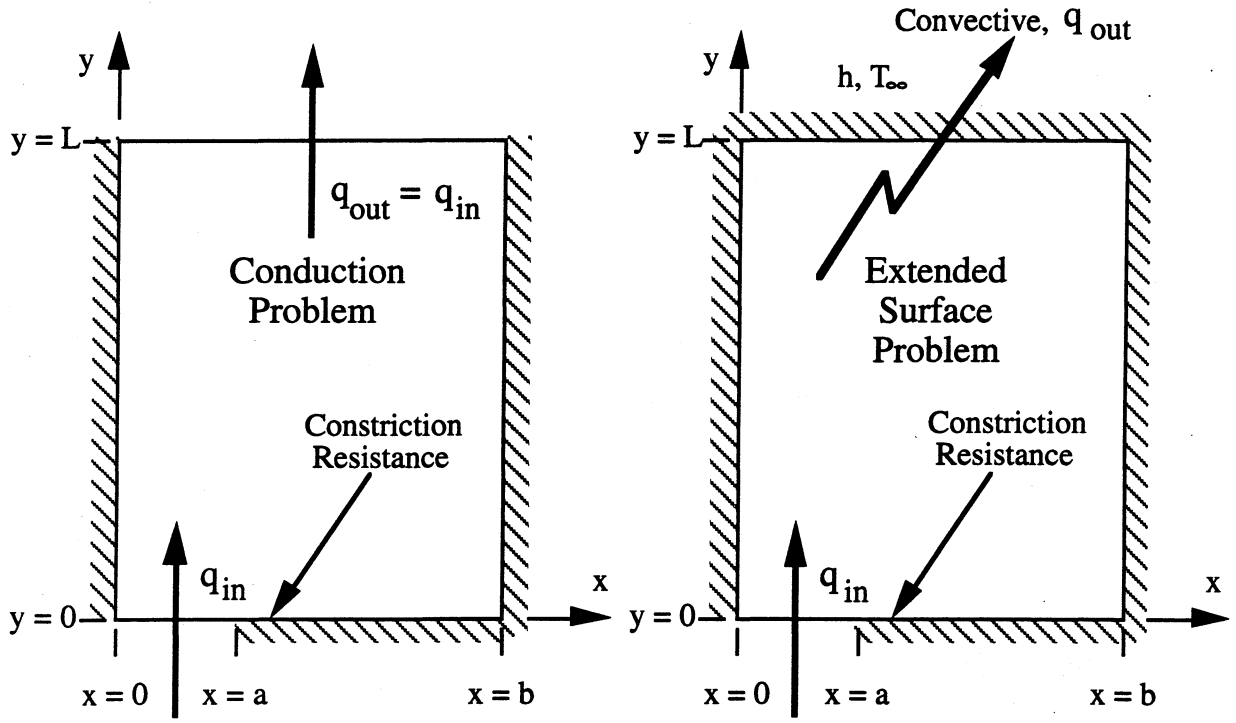

Figure 2.4. Symmetrical Sections of the Two Problems Investigated

constriction resistance takes the form:

$$R_c^* = \frac{R_c}{R_p} = \frac{\frac{\Delta T}{q} - \frac{L}{kA}}{\frac{L}{kA}} \tag{2.6}$$

where A is the cross sectional area. Equation (2.6) reduces to:

$$R_c^* = \frac{kA\Delta T}{qL} - 1 \tag{2.7}$$

For the extended surface problem, the dimensionless constriction resistance takes the form:

$$R_c^* = \frac{R_c}{R_p} = \frac{\frac{1}{h A_s \eta} - \frac{1}{h A_s \eta_p}}{\frac{1}{h A_s \eta_p}} \tag{2.8}$$

where A_s is the extended surface area and η_p is the perfect contact efficiency ($\eta_p = \frac{\tanh(m)}{m}$ for this geometry). Equation (2.8) reduces to:

$$R_c^* = \frac{\tanh(m)}{m\,\eta} - 1 \tag{2.9}$$

After solving the conduction problem and the extended surface problem (for fin parameters of 3.0 and 0.75) numerically over a range of constriction ratios, the vast differences between the dimensionless constriction resistances is clear, see Figure 2.5. Hence, "fin" studies made without the convective boundary condition on the fin surfaces generally can not be applied to plate-fin heat exchanger designs. Thus, an investigation into the influence of macroscopic heat flow constrictions on fin/tube heat exchanger performance is clearly needed.

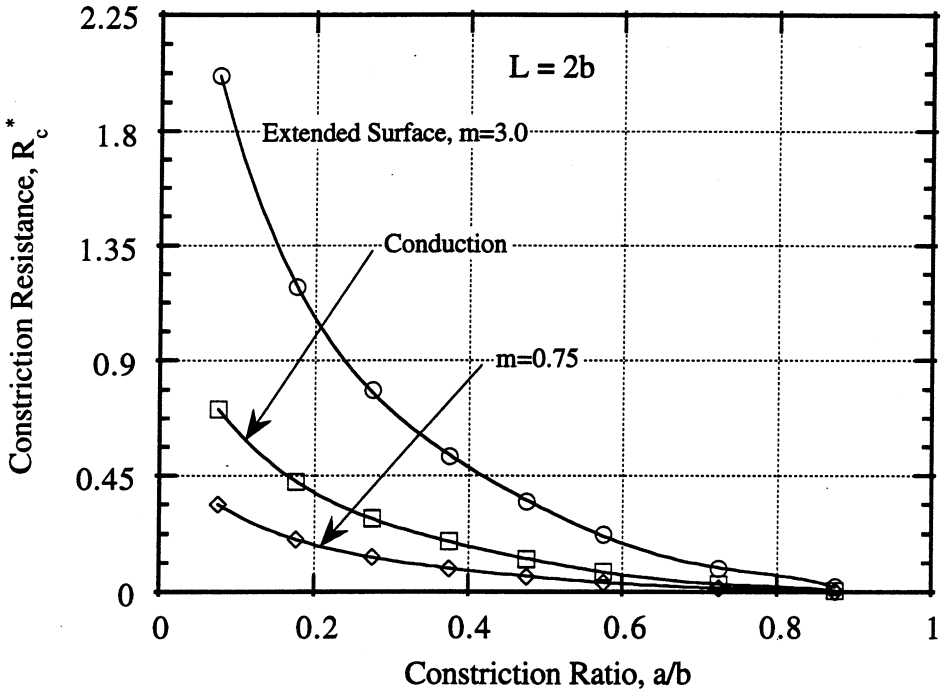

Figure 2.5. Influence of Constriction Ratio on Constriction Resistance for a Conductive Plate-Fin and Extended Surface Plate-Fin

3. REPRESENTATIVE GEOMETRIES

3.1 Assumptions and Boundary Conditions

The following assumptions and boundary conditions are consistent with all representative geometries analyzed during this investigation. A more specific description of each geometry shall follow these general conditions.

All fins are assumed to made out of an isotropic and homogeneous material; the thermal conductivity of the fin is considered to be uniform and independent of temperature. In addition, it is assumed that no energy is generated within the fin and that the heat transfer coefficient is constant along the surface of the fin. All interstitial substances are assumed to be stagnant, isotropic and homogeneous substances with constant thermal conductivity. Ambient and boundary temperatures are also assumed to be constant quantities. Collared and non-collared, plate-fin geometries are assumed to only have two dimensional heat flow within the fin.

All fin edges are considered adiabatic boundaries for the representative geometries. Perfect contact is assumed at the macroscopic contact areas along the fin/tube interface. The non-contact boundary at the interface is either considered adiabatic or having conductive heat flow through an interstitial substance of constant thickness. Convective heat flow from the extended surface is always present.

3.2 Analysis of Non-Collared Plate-Fins

The non-collared plate-fin is the first extended surface examined. A typical rectangular, plate-fin cross section (from an evaporator supplied by Peerless of America, Inc.) was used in order to obtain a realistic estimate of fin area, tube diameter and magnitude of fin thickness for modeling a representative geometry. Figure 3.1 illustrates the cross section used while Figure 3.2 depicts the two dimensional, representative geometry. Note that the non-contact gaps are greatly exaggerated in these figures and a symmetric, annular estimation of the rectangular area of the typical fin was used in generating the geometry. In other words, the fin area in Figure 3.2 is approximately one fourth of the fin area in Figure 3.1. In addition, two other geometries similar to that of Figure 3.2 were also modeled. Figure 3.2 is consistent with Figure 3.1 such that three macroscopic contact spots has been simulated. Such contact at the fin/tube interface in now defined as three point contact. One and two point contacts are also examined (figures 3.3 and 3.4, respectfully) in an effort to determine the influence of contact location.

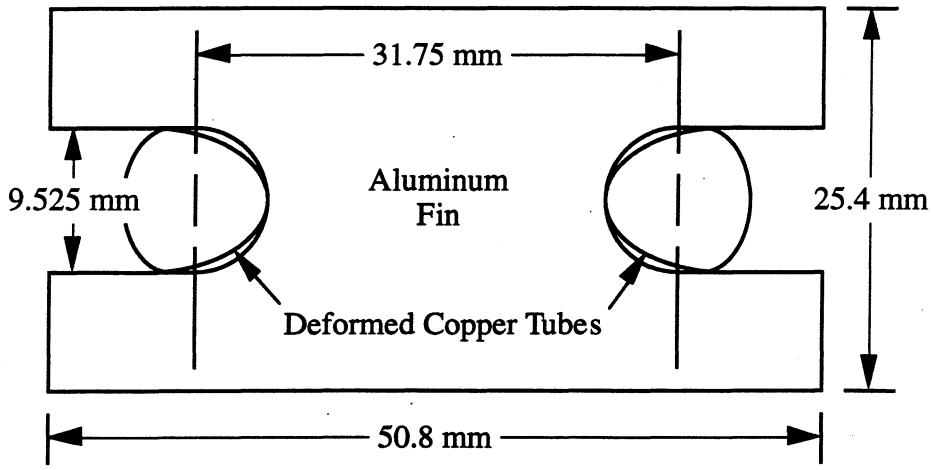

Figure 3.1. Typical Rectangular, Plate-Fin Cross Section

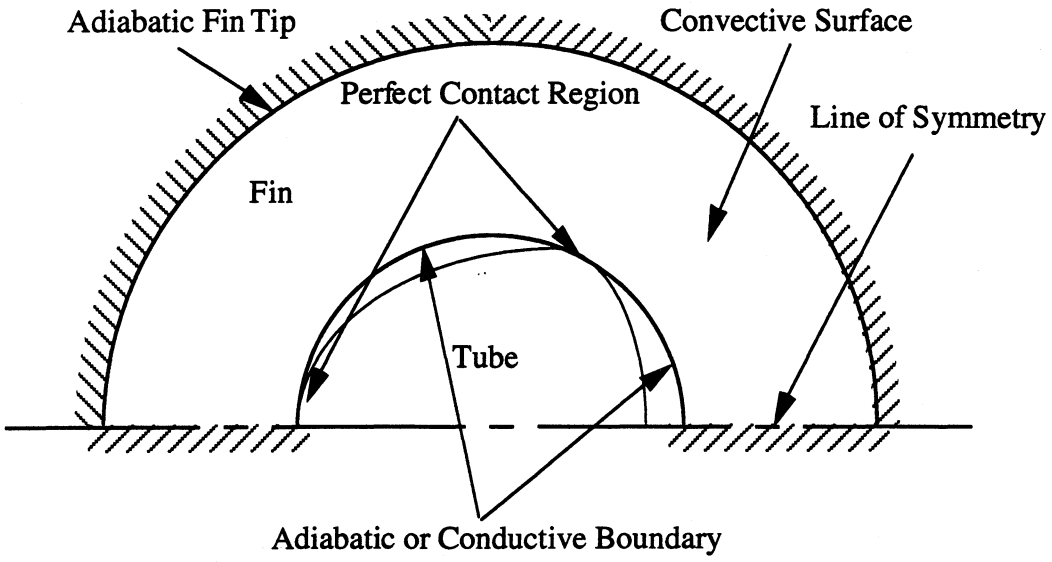

Figure 3.2. Representative Geometry of Non-Collared Plate-Fin (Three Point Contact)

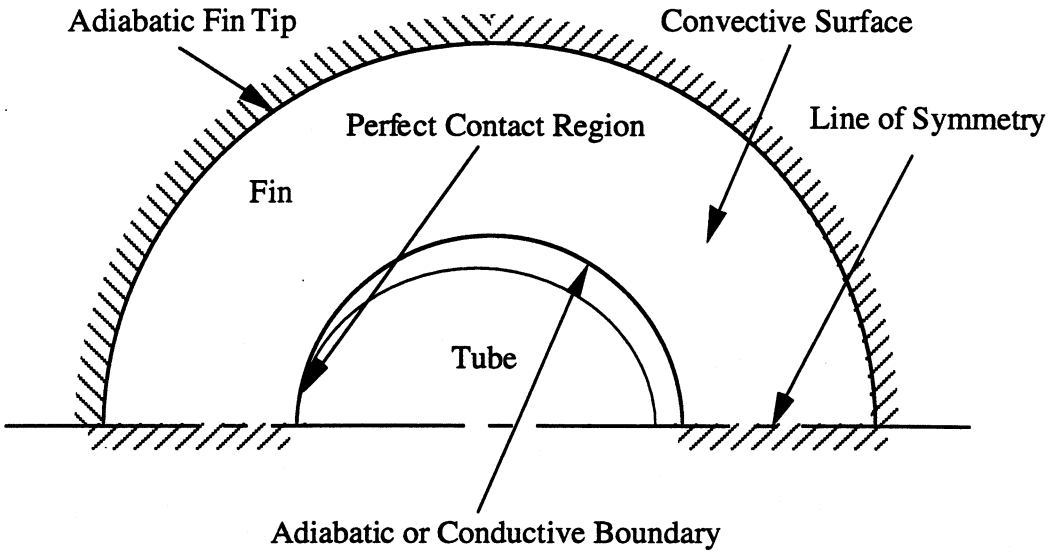

Figure 3.3. Representative Geometry of Non-Collared Plate-Fin (One Point Contact)

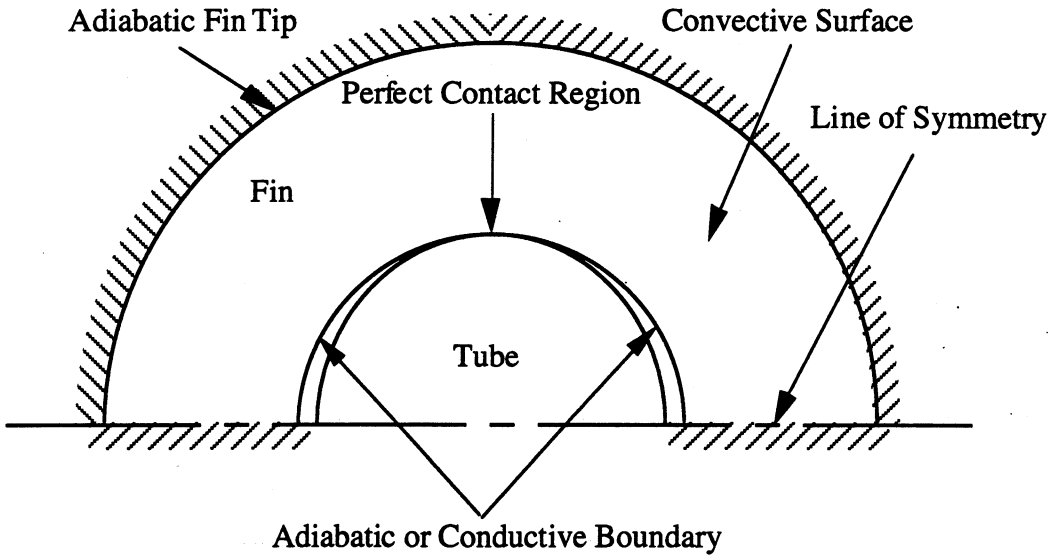

Figure 3.4. Representative Geometry of Non-Collared Plate-Fin (Two Point Contact)

3.3 Analysis of Non-Collared Plate-Fins with Frost Buildup

The second extended surface analyzed in this investigation is the non-collared plate-fin with frost buildup. A two dimensional, rectangular geometry was selected to examine the shunting of heat flow through a small frost buildup around the base of the fin (the fin not being in direct contact with the tube wall). Since the frost buildup could entrap air or condensation in the gap during frost formation, the influence to heat flow through each of the three substances are investigated. Figure 3.5 illustrates a symmetrical section of the representative geometry; once again, some of the fin dimensions are modeled after Figure 3.1 (magnitude of fin thickness and height). An adiabatic boundary condition along the frost surface was assumed specifically for this geometry.

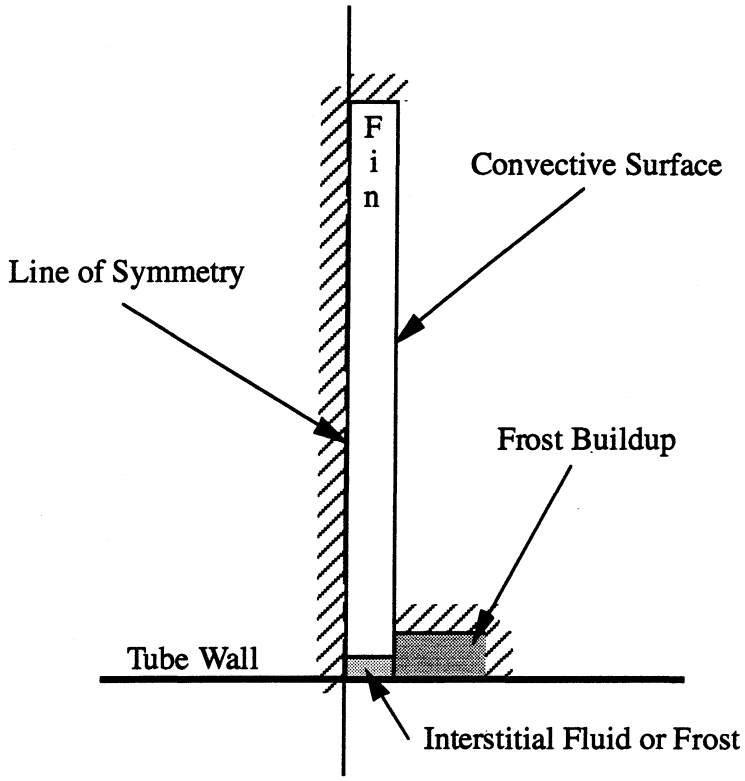

Figure 3.5. Representative Geometry of Non-Collared Plate-Fin with Frost Buildup

3.4 Analysis of Collared Plate-Fins

The final extended surface examined in this investigation is the collared plate-fin. The two dimensional geometry of Figure 3.3 (illustrating the radial and azimuthal directions) was simply expanded in order to represent a two dimensional heat flow, in the axial and azimuthal directions, at the fin base; Figure 3.6 depicts this representative geometry. The constant gap between the

collar and tube is assumed to be fluid or frost filled and the outer surface of the collar is assumed adiabatic. The exact length of the collar is specified by the number of fins per meter (fins per inch) from the heat exchanger of interest.

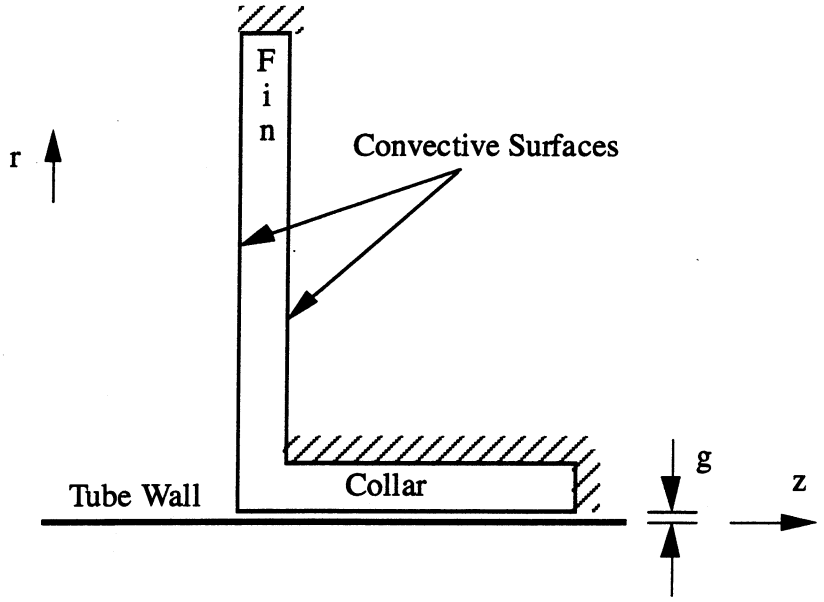

Figure 3.6. Representative Geometry of Collared Plate-Fin (Radial and Axial Directions)

4. DEFINITION OF DIMENSIONLESS PARAMETERS

4.1 Fin Parameter

The thermal performance of an extended surface is a strong function of the fin parameter, m; which takes the following form when based on tube radius:

$$m_b = \left[\frac{h\, r_b^2}{k_{al}\, \delta}\right]^{\frac{1}{2}} \tag{4.1}$$

Note that m^2 is a ratio of the conductive resistance of the fin, $\frac{L}{k\,(\delta W)}$, to the convective resistance between the fin and the fluid, $\frac{1}{h\,(WL)}$. The fin parameter may also be based on the characteristic length of the extended surface, $r_t - r_b$, such that it takes the form:

$$m_l = \left[\frac{h\,(r_t - r_b)^2}{k_{al}\, \delta}\right]^{\frac{1}{2}} \tag{4.2}$$

The dramatic effect of m_b on fin performance can be shown by analyzing the two point annular geometry shown in Figure 4.1. Assuming an adiabatic boundary condition at the fin/tube

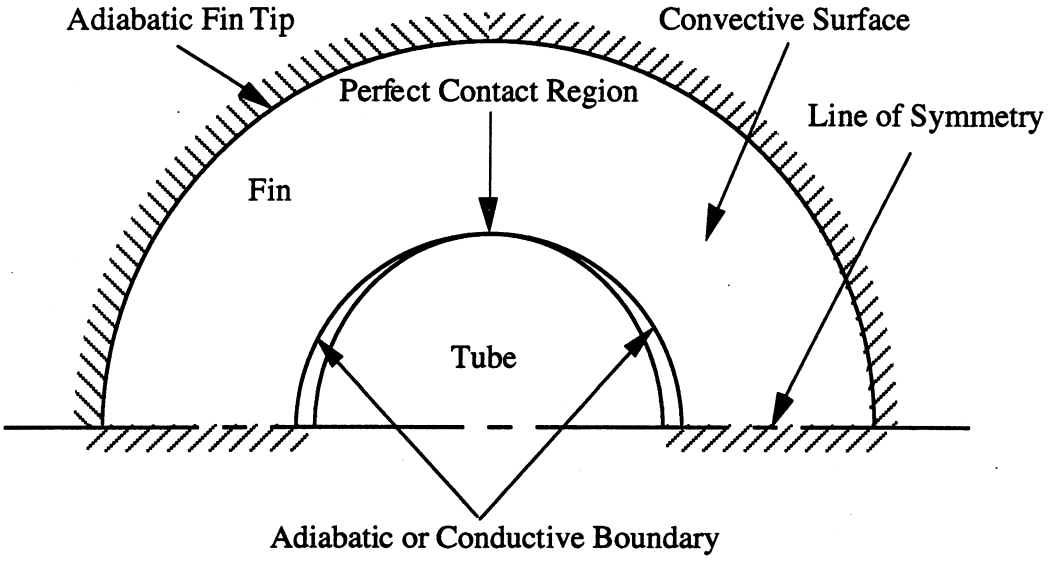

Figure 4.1. Representative Geometry of Non-Collared Plate-Fin (Two Point Contact)

interface over the non-contact portion and given a tip to base radius ratio of 4 and various m_b of 0.1, 0.25, 0.5 and 1.0, the fin efficiency, η, as a function of constriction ratio, a/b, can be numerically determined as illustrated in Figure 4.2. It is logical that a fin would become

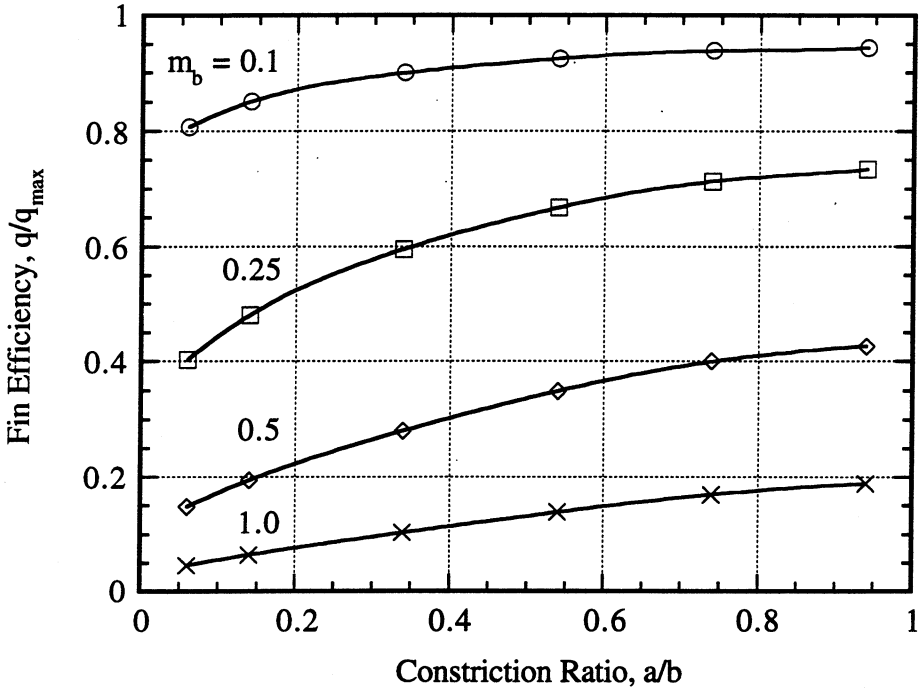

Figure 4.2. Influence of Fin Parameter on Fin Efficiency for Various Constriction Ratios

isothermal at the base temperature, i.e. $\eta = 1$, as: its conductivity or thickness became large, the convective heat transfer coefficient approached zero or the conductive path approached zero, meaning the base radius becoming small with r_t / r_b fixed at a finite value. On the other hand, a fin would become isothermal at the ambient temperature, i.e. $\eta = 0$, if: the fin conductivity was extremely poor, the fin was extremely thin, the convective heat transfer coefficient was large or the conductive path became very extended, meaning the base radius becoming extremely large with r_t / r_b fixed at a finite value. Thus, as long as r_t / r_b is finite, the following limits apply:

$$m_b \to 0 \Rightarrow \eta \to 1; \; m_b \to \infty \Rightarrow \eta \to 0 \qquad (4.3a,b)$$

for all constriction ratios.

The fin parameter, for the straight fin of rectangular profile used in studying non-collared plate-fins with frost buildup, see Figure 4.3, is defined as:

$$m_r = \left[\frac{h L_f^2}{k_{al}\,\delta}\right]^{\frac{1}{2}} \tag{4.4}$$

Using an equivalent fin parameter, m_e, based on the characteristic length $L_f = r_t - r_b$, the annular and rectangular fins may be compared where:

$$m_e = \left(\frac{r_t}{r_b} - 1\right) m_b \tag{4.5}$$

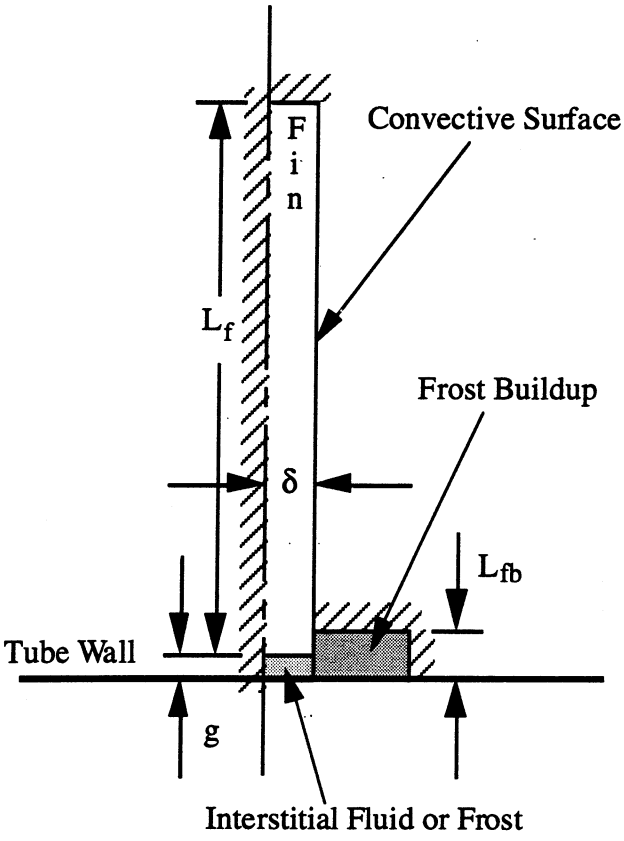

Figure 4.3. Representative Geometry of Non-Collared Plate-Fin with Frost Buildup

4.2 Interstitial Conductance Parameter

In order to better analyze the influence of interstitial substances, it was desirable to develop meaningful dimensionless parameters which would give an indication of their relative contribution

to fin performance over a range of gap thicknesses. The variables used in the derivations are defined in Figure 4.4. Assuming 1-D heat flow across a gap of constant thickness, the resistance

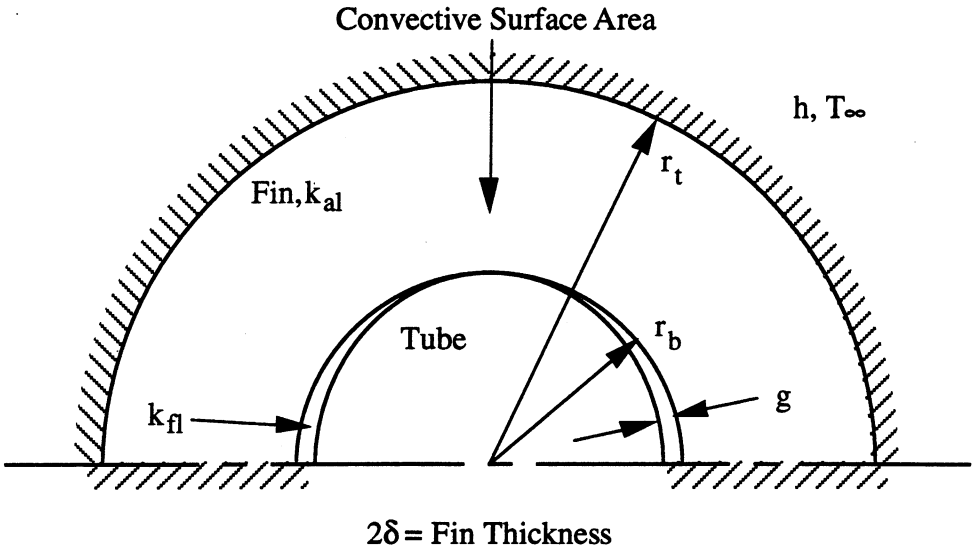

Figure 4.4. Variables Used in Interstitial Conductance Parameter Derivation

for the radial conduction across the gap is:

$$R_g = \frac{g}{k_{fl}(2\,\delta)(2\pi\, r_b)} \tag{4.6}$$

since $g << r_b$. We now nondimensionalize by the resistance of the conductive path through the fin:

$$R_{cond} = \frac{(r_t - r_b)}{k_{al}(2\delta)(2\pi\, r_b)} \tag{4.7}$$

where $r_t - r_b$ is used a the characteristic length, to arrive at:

$$R^*_{g,cond} = \frac{k_{al}}{k_{fl}} \frac{g}{(r_t - r_b)} \tag{4.8}$$

Defining the dimensionless interstitial conductance, based on the conductance of the fin, as the inverse of $R^*_{g,cond}$ we finally have:

$$H_{g,cond} = \frac{k_{fl}}{k_{al}} \frac{(r_t - r_b)}{g} \tag{4.9}$$

Equation (4.6) may also be nondimensionalized by the resistance of the convective path between the fin and the surrounding fluid, defined as:

$$R_{conv} = \frac{1}{h A_s} \tag{4.10}$$

where the surface area, A_s, is defined using the same characteristic length, that is:

$$A_s = 4\pi r_b (r_t - r_b) \tag{4.11}$$

Hence, the dimensionless interstitial conductance, based on the convective conductance, is:

$$H_{g,conv} = \frac{k_{fl} \delta}{g h (r_t - r_b)} \tag{4.12}$$

For simplicity, $H_{g,conv}$ defined above shall be refered to as H_{gl}.

It is now of interest to establish the relation between both interstitial parameters. Realizing that these parameters differ only by the resistance ratio of the conductive and convective paths, we can write:

$$\frac{R_{cond}}{R_{conv}} = \frac{h (r_t - r_b)^2}{k_{al} \delta} \tag{4.13}$$

where the right hand side is m_l^2 defined in Equation (4.2). As a result, we have:

$$H_{g,cond} = H_{gl} m_l^2 \tag{4.14}$$

Similarly, for the straight fin of rectangular profile used in studying non-collared plate-fins with frost buildup we have the following interstitial conductance parameters:

$$H_{g,cond} = \frac{k_{fl} L_f}{k_{al} g};\ H_{g,conv} = \frac{\delta k_{fl}}{g h L_f} \qquad (4.15a,b)$$

and a comparable relation to Equation (4.14):

$$H_{g,cond} = H_{g,conv} m_r^2 \qquad (4.16)$$

where m_r^2 is defined by Equation (4.4). Again for simplicity, $H_{g,conv}$ defined in Equation (4,15b) shall be refered to as H_{g2}.

The following relations between the interstitial conductance limits and the boundary condition at the fin/tube interface, for the non-contact regions, may be inferred from equations (4.9), (4.12) and (4.15a,b):

$$H_g \rightarrow 0 \Rightarrow \text{adiabatic};\ H_g >> 1 \Rightarrow \text{perfect contact may be assumed} \qquad (4.17a,b)$$

In addition, the interstitial resistance is dominant over either the conductive or convective path resistances when $H_g < 1$; on the other hand, it is less dominant when $H_g > 1$. Figure 4.5 fully illustrates these relations for three constriction ratios of the fin geometry in Figure 4.1, with a fin parameter of 0.25 and a tip to base radius ratio of 4.

4.3 Range of Parameter Values

In order to perform an investigation of the title problem, it is necessary to use a representative range of fin and interstitial conductance parameters, tip to base radius ratios and fin densities (for collared fin geometries). In turn, these parameters and ratios are determined by either selecting, measuring or calculating representative quantities for their dependent variables.

Representative values for the convective heat transfer coefficient, tube radius, fin thickness and fin thermal conductivity were necessary in establishing a fin parameter range for all geometries. A convective heat transfer coefficient of 45 W/m^2-K was established by using dimensions from a typical plate-fin evaporator (supplied by Peerless of America, Inc.) and experimental results from Shepherd (1956) for a similar coil. This value was also confirmed from experimental results by Rich (1975). This quantity was then divided by 2 and multiplied by 2 in order to establish a minimum (22.5 W/m^2-K) and maximum (90 W/m^2-K) heat transfer coefficient used in calculating a fin parameter range. Typical tube radii of 3.18 mm (0.125 in) to 9.53 mm (0.375 in) were ascertained from Wood et al. (1987). Fin thicknesses from 0.1016 mm (0.004 in) to

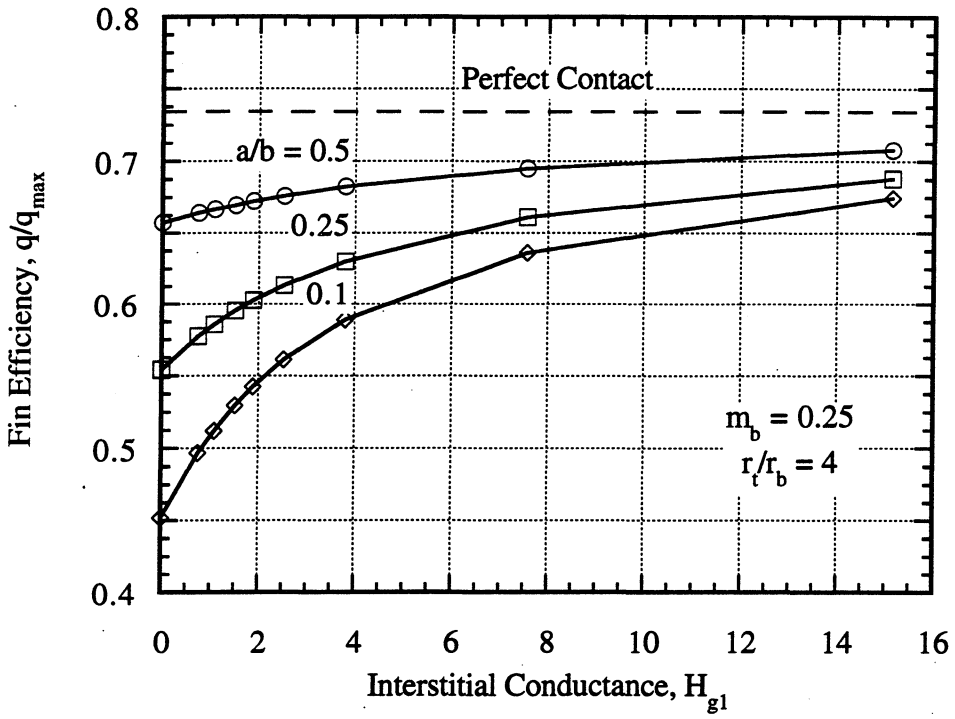

Figure 4.5. Influence of Interstitial Conductance Parameter on Fin Efficiency

0.254 mm (0.01 in) were standard test sizes for Sheffield et al. (1985, 1989) and Nho and Yovanovich (1989). Finally, a specific thermal conductivity for an aluminum fin was assumed 170 W/m-K from Incroperia and DeWitt (1990).

Along with the representative values of convective heat transfer coefficients, base radii and fin thicknesses, other standard quantities for gap thickness and interstitial thermal conductivity were required in establishing a representative interstitial conductance parameter range. In addition, tip to base radius ratios were necessary for the annular geometries while a frost buildup to gap thickness ratio was necessary for the straight fin of rectangular profile. Gap thicknesses were assumed to be in the range of 0.00254 mm (0.0001 in) to 0.0508 mm (0.002 in). The thermal conductivities of the interstitial fluids of water and air were taken to be 0.56 and 0.024 W/m-K (Incroperia and DeWitt, 1990), respectfully. The thermal conductivity of frost was found to lie within the above range, approximately 0.13 W/m-K (Dietenberger, 1983). Tip/base radius ratios were assumed to be within 2 and 5 (measured coil had a ratio of 4). Finally, the ratio of frost/gap thickness was arbitrarily taken to be less than 25.

A range of fin densities was also required for the collared fin analysis. Standard fin spacings of 236 fins per meter (6 fins per inch), 551 fins per meter (14 fins per inch) and 787 fins per meter (20 fins per inch) used by Ernest et al. (1985) and Sauer and Sheffield (1987) in experimental programs were employed.

After obtaining the representative values for the variables of the fin and interstitial conductance parameters, minimum and maximum values were calculated in order to investigate relevant heat exchangers. Both parameter ranges varied slightly between the annular geometries (collared and non-collared) and the rectangular geometry (non-collared with frost buildup).

From Equation (4.1), the fin parameter for the annular plate-fins ranged from 0.10 to 0.97. Using Equation (4.12), the interstitial conductance parameter ranged from 0 to 150. Similarly, the fin parameter for the straight fin of rectangular profile ranged from 0.10 to 1.0 (Equation 4.4) and the interstitial conductance parameter ranged from 0 to 150 (Equation 4.15b).

4.4 Baseline Case Defined

The following reference or baseline case is now defined in order that the influence of specific parameters or ratios may be examined individually, while keeping the others constant. For the annular geometries:

$$m_b = 0.25;\ \frac{r_t}{r_b} = 4;\ H_{g1} = 0;$$
$$551 \text{ fins/meter (collared geometry)} \qquad (4.18a,b,c,d)$$

Two point contact is used for the non-collared baseline case, while one point contact is always assumed for the collared geometry.

For the straight fin of rectangular profile (non-collared plate-fin with frost buildup):

$$m_e = 0.75;\ \text{Frost/Gap Thickness} = 0 \qquad (4.19a,b,c)$$

Once again, these values are based on a typical plate-fin evaporator mentioned earlier in this chapter.

5. NUMERICAL METHOD

5.1 Development of Finite-Difference Equations

Although an analytical, i.e. exact, solution to the extended surface problems of the title investigation is desired, complex fin geometries (such as a collared fin) and mixed boundary conditions (most evident at the fin/tube interface) prevent such problems from being solved. For these cases, some type of numerical, or finite-difference, techniques must be effected. The finite-difference method replaces the continuous geometry and independent variables by a discrete grid network; thus, a continuous change of the dependent variable is no longer given by the solution, but rather it yields its value at a finite number of discrete grid points distributed throughout the region (see Clausing, 1988).

Finite-difference equations are commonly developed from an energy balance on the control volume about the nodal point. Such a control volume is illustrated in Figure 5.1. Since a majority of this investigation deals with annular geometries, examples within this chapter will be

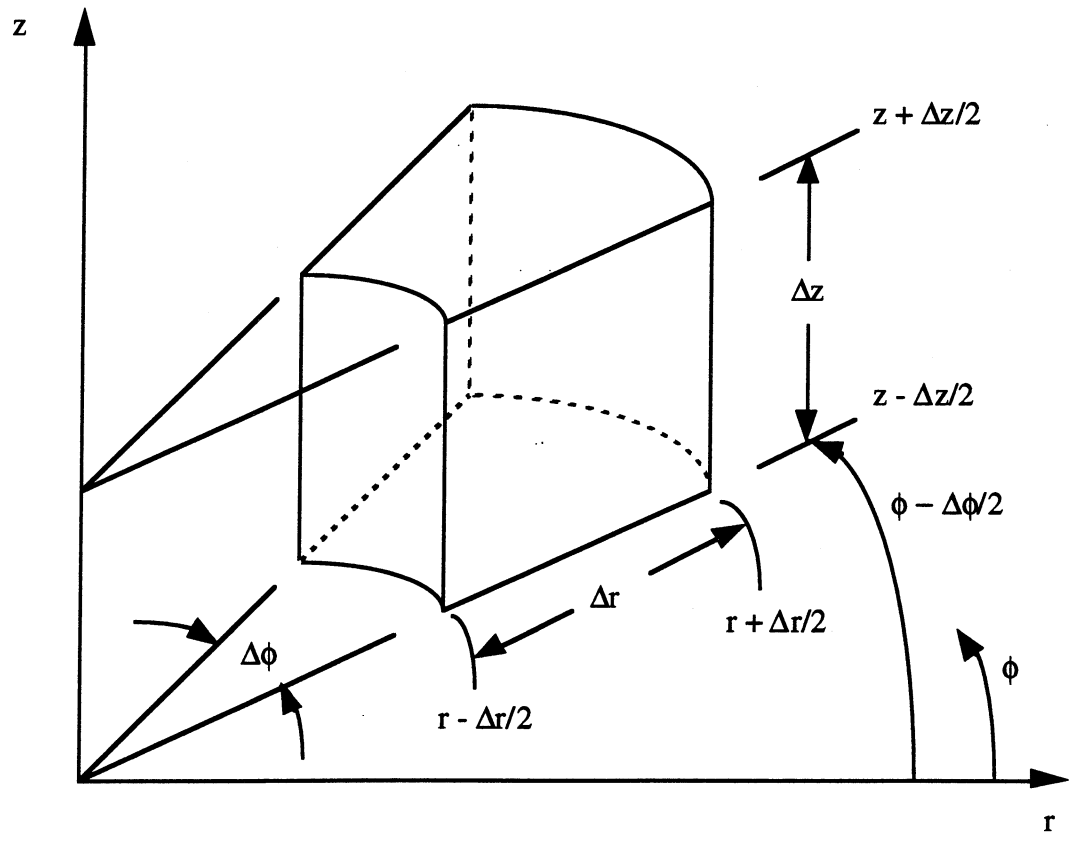

Figure 5.1. Control Volume Element in Cylindrical Coordinates

in cylindrical coordinates. It now becomes necessary to define a coordinate system such that an energy balance can be written. For simplicity, the discussion of finite-difference equation development shall now be limited to two dimensions, where Δz in Figure 5.1 would simply be the fin thickness. However, the techniques described in this chapter are easily extended to three dimensions.

First, let us define a coordinate system such that:

$$r_i = i(\Delta r)$$
$$\phi_j = j(\Delta \phi)$$

where r_i represents the radial distance to the ith node and ϕ_j represents the azimuthal angle to the jth node. Energy exchange involving an interior control volume about the node (i,j) is influenced by the conduction from the adjacent nodes and convection from the surfaces. Figure 5.2 illustrates the exchange. Since the actual direction of heat flow from the surrounding nodes and

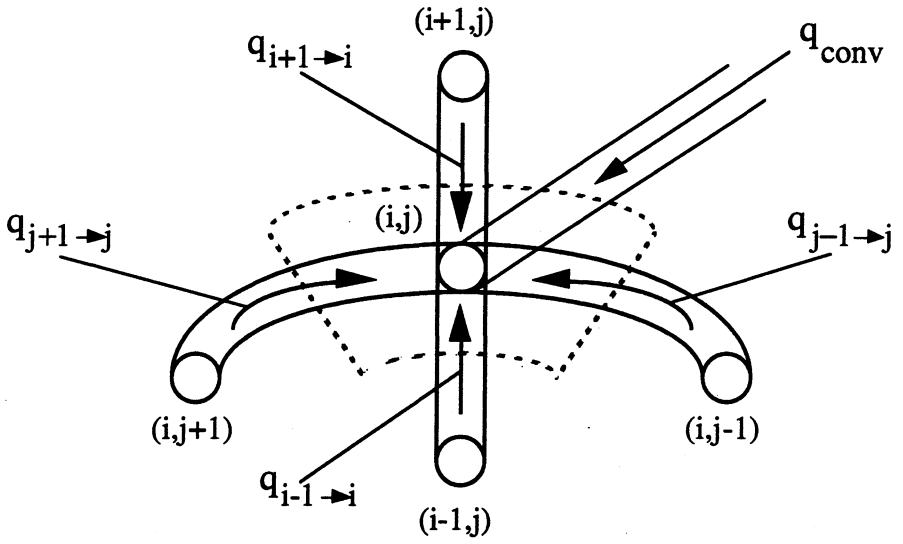

Figure 5.2. Heat Flow Into the Control Volume About Node (i,j)

the convective fluid are not known, the energy balance is formulated by assuming all heat flow is into the node. The correct finite-difference equation is obtained if the heat equations are expressed in a consistent way. Equation (5.1) is the energy balance for Figure 5.2 based on

Fourier's law, using an algebraic approximation for the temperature gradient at the boundaries of the control volume, and Newton's law of cooling.

$$\frac{k_{al}\left(r_i - \frac{\Delta r}{2}\right)\Delta\phi\, 2\delta\,(T_{i-1,j} - T_{i,j})}{\Delta r} + \frac{k_{al}\left(r_i + \frac{\Delta r}{2}\right)\Delta\phi\, 2\delta\,(T_{i+1,j} - T_{i,j})}{\Delta r}$$
$$+ \frac{k_{al}\,\Delta r\, 2\delta\,(T_{i,j-1} - T_{i,j})}{r_i\,\Delta\phi} + \frac{k_{al}\,\Delta r\, 2\delta\,(T_{i,j+1} - T_{i,j})}{r_i\,\Delta\phi} + 2\,h\,\Delta r\left(r_i\,\Delta\phi\right)(T_\infty - T_{i,j}) = 0 \qquad (5.1)$$

Similar equations (or types) are derived for nodes at the fin/tube interface and the perimeter of the fin. Introducing dimensionless variables:

$$T^* = \frac{T - T_\infty}{T_b - T_\infty};\ \Delta r^* = \frac{\Delta r}{r_b};\ m_b^2 = \frac{h\, r_b^2}{k_{al}\,\delta} \qquad (5.2a,b,c)$$

Equation (5.1) becomes:

$$d_i\, T^*_{i-1,j} + f_i\, T^*_{i+1,j} + \lambda\, T^*_{i,j-1} + \lambda\, T^*_{i,j+1} - \left[2 + 2\lambda + m_b^2\,\Delta r^{*2}\right] T^*_{i,j} = 0 \qquad (5.3)$$

where:

$$d_i = \left(1 - \frac{\Delta r}{2r_i}\right);\ f_i = \left(1 + \frac{\Delta r}{2r_i}\right);\ \lambda = \left[\frac{1}{(i\Delta\phi)^2}\right] \qquad (5.4a,b,c)$$

Equation (5.3), along with the corresponding equations for the boundary nodes are of a form such that an iterative scheme can be used to solve the set of algebraic equations.

5.2 Extrapolated Liebmann Method

Since cyclic iterative methods are efficient and easily programmed for digital computation, a single step (new temperature values are used when available) iteration method, called the Extrapolated Liebmann method, was effected. When the Liebmann method is applied to Equation (5.3), the process becomes:

$$T^*_{i,j} = (1 - \omega)\, T^*_{i,j} + \beta\left(d_i\, T^*_{i-1,j} + f_i\, T^*_{i+1,j} + \lambda\, T^*_{i,j-1} + \lambda\, T^*_{i,j+1}\right) \qquad (5.5)$$

where:

$$\beta = \left(\frac{\omega}{2 + 2\lambda + m_b^2 \Delta r^{*2}} \right) \tag{5.6}$$

The relaxation parameter, ω, takes on values of $1 < \omega < 2$ in order to accelerate the convergence process (overrelaxation). If $\omega \geq 2$ then the size of the residual, the difference between the left and right hand sides of Equation (5.5), would remain the same or increase resulting in divergence. If $\omega < 1$, the iteration would be underrelaxed; this is undesirable for linear governing equations since convergence would be slow. An optimum ω value is desired for maximum convergence and is usually determined by trial and error. For this investigation, a relaxation parameter of approximately 1.95 proved the most effective.

Theoretically, an infinite number of iterations would be required for an exact solution; however, an energy balance over the entire fin is used to terminate the iterative process. When the percent error between the heat rate in and the heat rate out falls below a user specified point, the iteration is ended. This in itself introduces some error to the process in addition to the error caused by the finite-difference representation. These errors are now analyzed in some detail.

5.3 Accuracy of Numerical Solution

Since the truncation error approaches zero as the spatial increments approach zero (this property is known as consistency), it can be minimized to an acceptable level by refining the grid mesh, assuming round-off error is relatively small; however, computational time is greatly increased. In using the numerical method described for this investigation, it was necessary to ascertain the grid size required for accurate results.

The numerical results will be compared with the exact solution of an annular fin with perfect contact at the fin/tube interface. The fin efficiency, η, for the case of perfect contact is:

$$\eta = \frac{-2\, m_b}{m_b \left[\left(\frac{r_t}{r_b} \right)^2 - 1 \right]} \left[\frac{K_1(m_t)\, I_1(m_b) - I_1(m_t)\, K_1(m_b)}{K_1(m_t)\, I_0(m_b) + K_0(m_b)\, I_1(m_t)} \right] \tag{5.7}$$

which is defined as the ratio of the actual heat flow rate from the fin to the heat flow rate if the fin had infinite thermal conductivity. Note that I and K are modified Bessel functions of the first and second kind respectfully, and the subscript denotes the order. Comparisons of the fin efficiency were made using Equation (5.7), perfect contact case, and results from the numerical solution with differing mesh sizes. Energy balances, for iteration termination, were within 0.05

percent error. A reasonable grid size of 60 nodes in the radial direction and 80 nodes in the azimuthal direction yielded a satisfactory truncation and round-off error of less than 0.5%.

Since a rectangular geometry is effected for the frost buildup investigation, a separate error analysis is necessary. In order to determine the accuracy of this code, an analytical efficiency for 1-D conduction through an interstice and fin was calculated and compared to the code results for zero frost buildup. Figure 5.3 illustrates the geometry of the fin problem solved. The Appendix

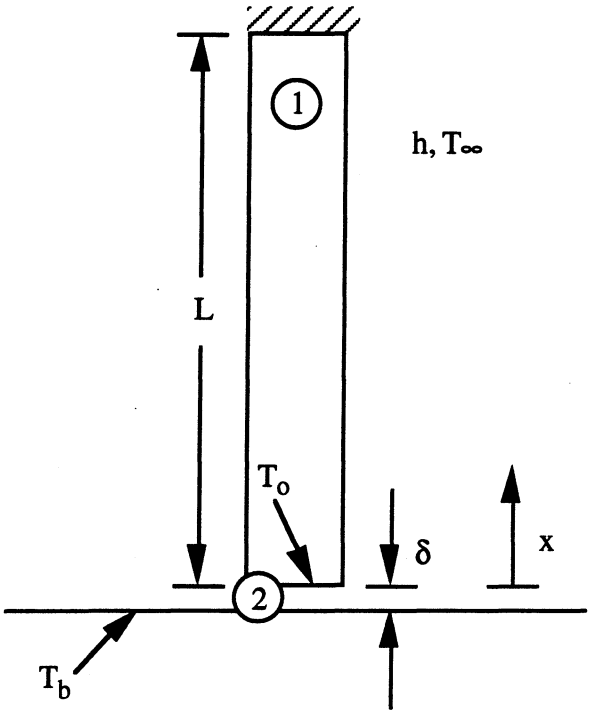

Figure 5.3. Fin Geometry for Analytical Solution

contains the details of the fin efficiency derivation, which is:

$$\eta = \frac{k_2 m_2^2 \tanh(m_1)}{k_1 m_1^2 \left[m_2^2 \delta^* \tanh(m_1) + m_1 \right]} \tag{5.8}$$

where:

$$\delta^* = \frac{\delta}{L};\ m_1^2 = \frac{h L^2}{k_1 \delta};\ m_2^2 = \frac{h L^2}{k_2 \delta} \qquad (5.9a,b,c)$$

and subscript 1 refers to the fin condition and subscript 2 refers to the interstitial condition.

Several cases, by varying the interstitial conductance, were run with no frost buildup to determine the accuracy of the code for the baseline case. A truncation and round-off error of less than 1.8% existed near adiabatic conditions ($H_{g2} << 1$), and less than 1% for conditions close to perfect contact ($H_{g2} >> 1$).

6. NUMERICAL RESULTS AND ANALYSIS

6.1 Non-Collared Plate-Fins

The influence of contact spot (location and number), tip/base radius ratio, fin parameter and interstitial conductance parameter on fin performance of non-collared plate-fins is examined. By deviating from a defined baseline case only by a single ratio or parameter, the magnitude of its influence on fin performance will be evident. The baseline case for the non-collared, plate-fin geometry is defined as:

$$m_b = 0.25;\ \frac{r_t}{r_b} = 4;\ H_{g1} = 0 \text{ (adiabatic non-contact interface)} \qquad (6.1)$$

Two point contact is also defined for this reference case. The fin parameter and tip/base radius ratio are based on a typical plate-fin, refrigerator evaporator supplied by Peerless of America, Inc.

The influence of one, two and three point contact, as defined in Chapter 3, on fin efficiency for a range of constriction ratios is illustrated in Figure 6.1. This graph shows the expected

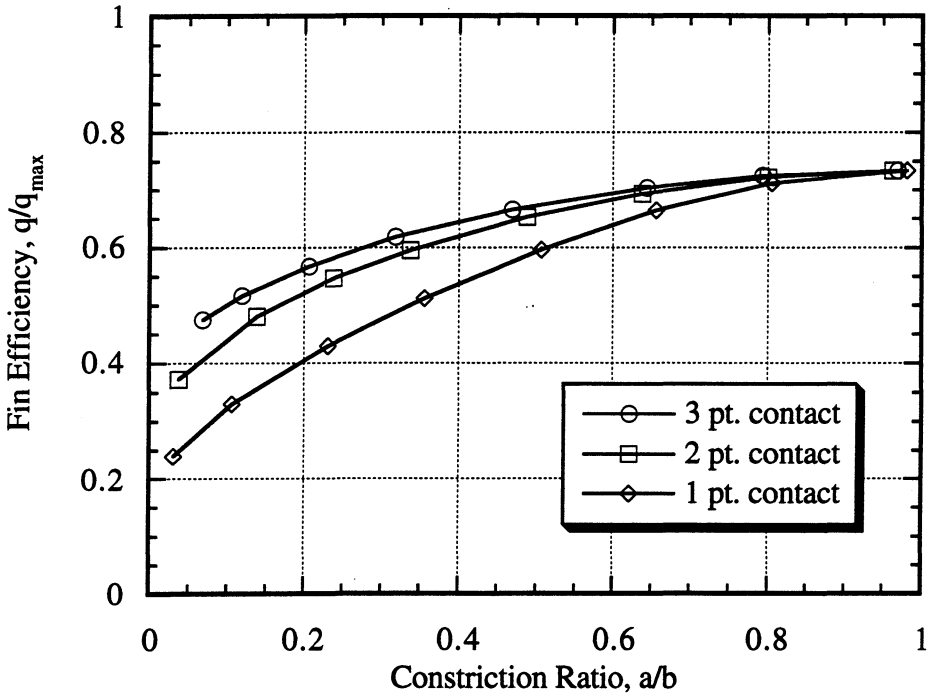

Figure 6.1. Influence of Number of Contacts and Total Contact Area on Fin Efficiency

deterioration in fin performance with a decrease in the number and area of the contact regions. This is due to larger temperature gradients (less temperature uniformity) within the fin as a result of uneven contact. This effect is especially severe with one point contact. For constriction ratios of less than 0.5, the difference in fin efficiency between three and one point contact is three times worse than between two and three point contact.

The fin efficiency values may be normalized by the perfect contact efficiency for any case in order to quickly determine the penalty of poor macroscopic conformity. The perfect contact efficiency for an annular fin is a function of the fin parameter, Equation (4.1), and the tip/base radius ratio and follows from Equation (5.7). The fin efficiencies, with perfect contact, for the complete range of fin parameters and tip/base radius ratios investigated are given in Table 6.1.

	Fin Efficiency, η			
m_b	$r_t/r_b = 2$	$r_t/r_b = 3$	$r_t/r_b = 4$	$r_t/r_b = 5$
0.10	0.9953	0.9775	0.9441	0.8960
0.25	0.9714	0.8753	0.7345	0.5891
0.50	0.8956	0.6464	0.4280	0.2876
1.00	0.6915	0.3435	0.1897	0.1191

Table 6.1. Perfect Contact Efficiency for Various Annular Fins

Figure 6.2 illustrates the influence of one, two and three contact points on the normalized fin efficiency. This graph not only shows the importance of good contact, but also how this contact is distributed. For example, at a constriction ratio of 0.2, a fin/tube interface with one contact point suffers a 45% loss in fin efficiency; however, with two or three contact points, the loss is only of 30 and 25% respectfully. In addition, efficiency losses are not only more severe with fewer contact points, but also occur at higher constriction ratios. A decrease in fin efficiency of greater than 10% is suffered with one point contact at constriction ratios less than 0.65. With two or three point contact, losses of greater than 10% occur with constriction ratios less than 0.5.

Because this variation in performance is caused by diverse temperature distributions within the fin, graphical representations are of interest. Figures 6.3, 6.4 and 6.5 show the temperature

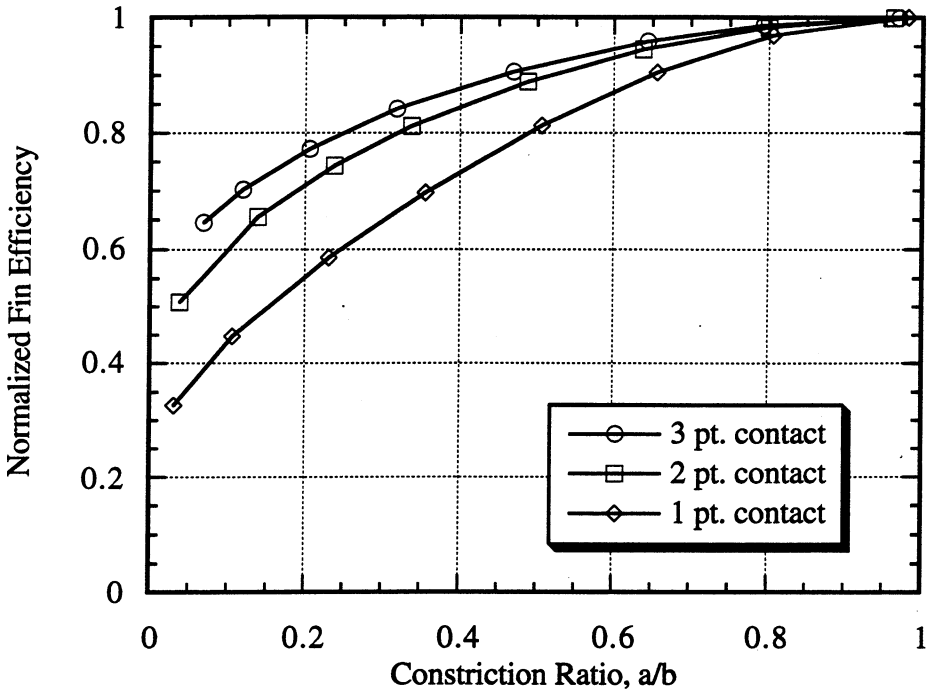

Figure 6.2. Influence of Number of Contacts and Total Contact Area on Normalized Fin Efficiency

distribution for one, two and three point contact, respectfully, of the baseline plate-fin geometry using a constriction ratio of 0.25. The darker shades represent temperatures closer to the tube temperature. Note that the temperature distribution of Figure 6.4 is not precisely symmetric about the vertical axis; this is due to an odd number of nodes in the azimuthal direction of the finite-difference code. This temperature distribution is symmetric about the horizontal axis.

Observing Figure 6.3, a singular contact point causes a large temperature difference between the fin/tube interface over a large portion of the non-contact region resulting in a normalized fin efficiency of approximately 60% (see Figure 6.2). Turning now to Figure 6.4, dividing the perfect contact region into two contact points shows a definite improvement in temperature uniformity within the fin. Consequently, an increase in normalized fin efficiency to 75% is evident. Finally, if contact occurs over three points, while still only having a constriction ratio of 0.25, the temperature difference across the non-contact interface is approximately uniform (referring to Figure 6.5). This results in a normalized fin efficiency of 80%.

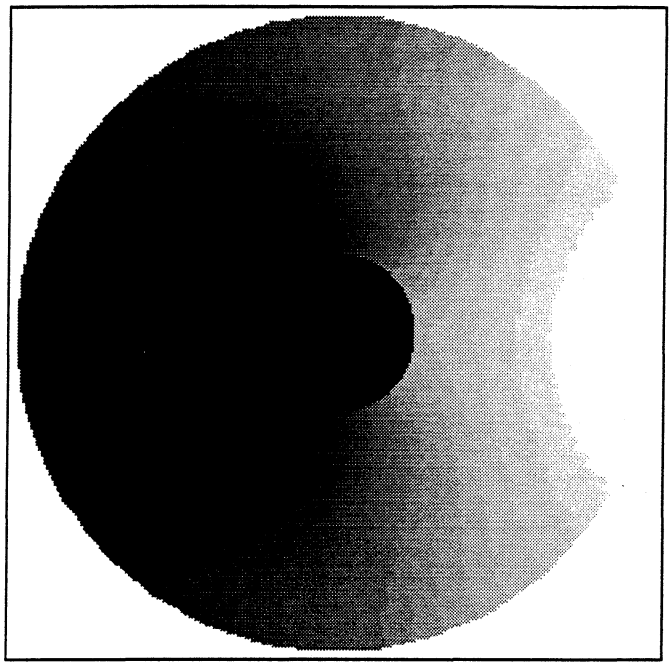

Figure 6.3. Temperature Distribution of the Baseline Case Annular Fin with One Point Contact (a/b = 0.25)

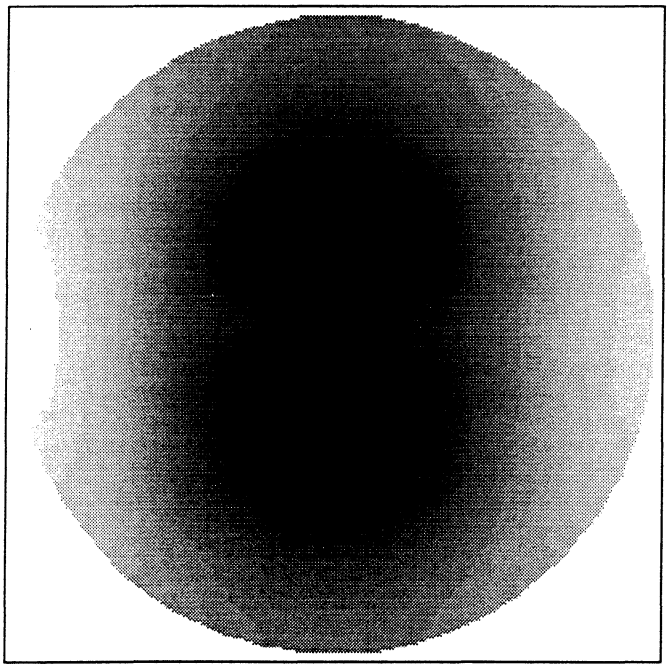

Figure 6.4. Temperature Distribution of the Baseline Case Annular Fin with Two Point Contact (a/b = 0.25)

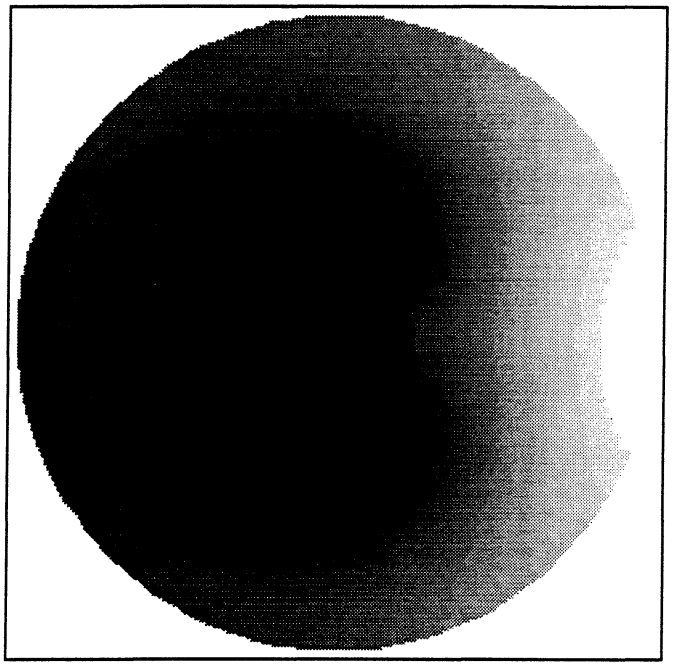

Figure 6.5. Temperature Distribution of the Baseline Case Annular Fin with Three Point Contact (a/b = 0.25)

Figure 6.6 illustrates the dramatic effect of various tip/base radius ratios (2, 3, 4 and 5) on the baseline case ($m_b = 0.25$) for all constriction ratios. This figure clearly shows the disadvantage of extending the conductive path of the fin, meaning increasing the base radius while fixing r_t/r_b at a finite value. For example, having $r_t/r_b = 3$ with a constriction ratio of 0.25 has approximately the same fin efficiency as having $r_t/r_b = 4$ with perfect contact. Note that while decreasing the r_t/r_b ratio, with m_b fixed, increases fin efficiency, the overall heat transfer rate decreases due to the diminished fin area. The problem becomes one of heat exchanger optimization; for this investigation, specific trends in fin efficiency, due to various tip/base radius ratios, are presented for constricted heat flow. Consider first the fin efficiency normalized by the perfect contact efficiency of Table 6.1 for $m_b = 0.25$. These results are displayed in Figure 6.7. Observing this figure, we see how increasing the tip/base radius ratio results in a more severe drop in normalized fin efficiency at lower constriction ratios. For example, at a constriction ratio of 0.1 and $r_t/r_b = 2$, the normalized fin efficiency is 85%, while at this same constriction ratio and $r_t/r_b = 5$, the normalized fin efficiency is 50%.

The influence of the fin parameter on the fin efficiency of the baseline case over all constriction ratios is depicted in Figure 6.8. Figure 6.9 illustrates the normalized fin efficiency dependence

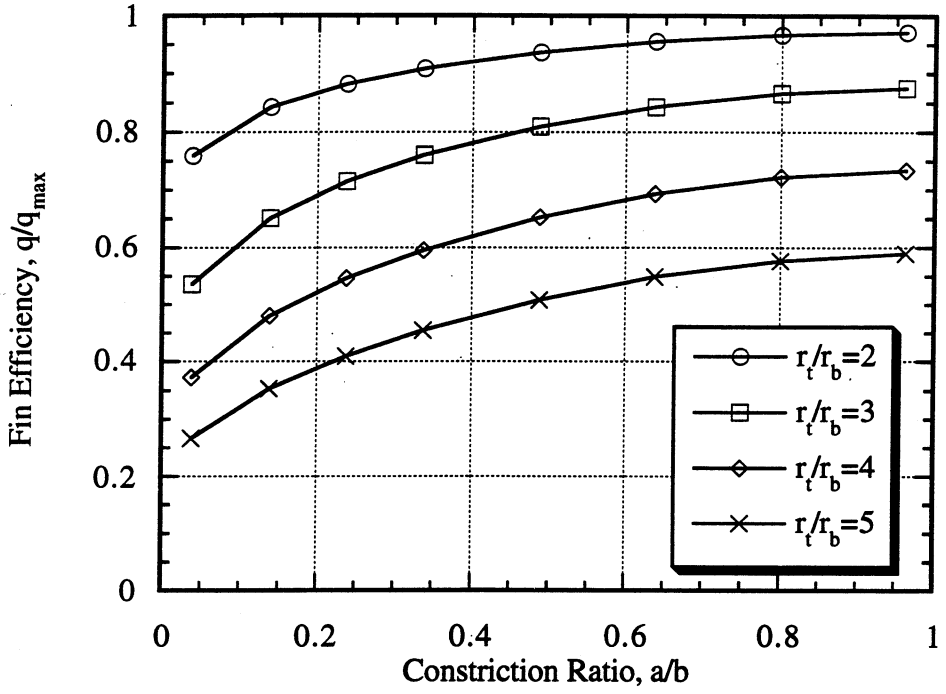

Figure 6.6. Influence of Tip/Base Radius Ratio on Fin Efficiency

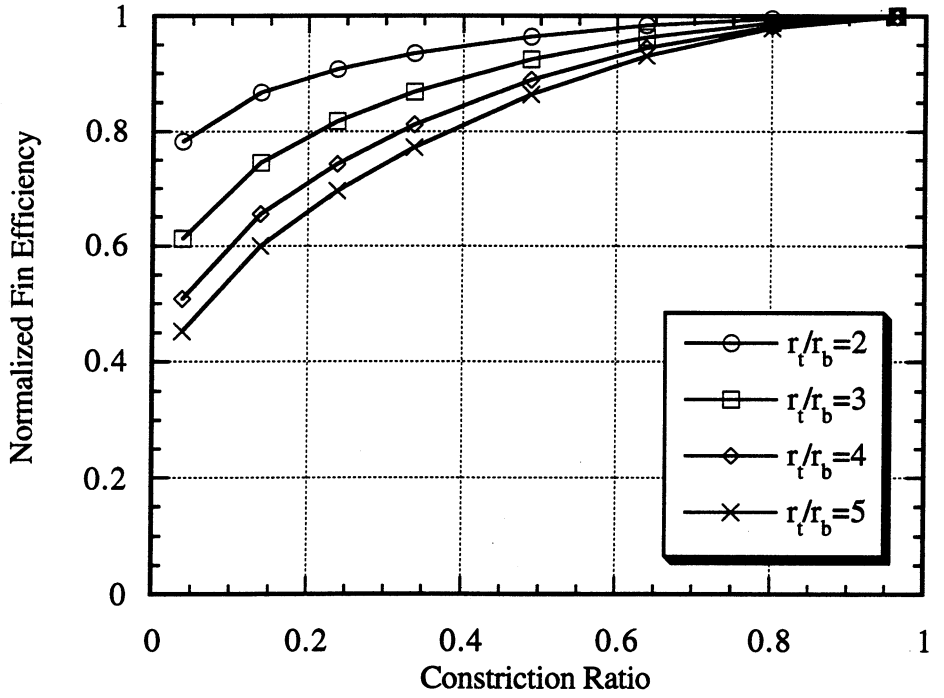

Figure 6.7. Influence of Tip/Base Radius Ratio on Normalized Fin Efficiency

on the fin parameter. The effect of varying the fin parameter on fin performance is very similar to the effect caused by varying the tip/base radius ratio. Commonly, poor contact at the fin/tube interface is alleviated by increasing the fin thickness. Often this is the easiest way to decrease the fin parameter; hence, to increase the fin efficiency. To illustrate this point, assume a constriction ratio of 0.1 and $m_b = 0.5$. Referring to Figure 6.8, forcing perfect contact or increasing fin thickness such that $m_b = 0.25$ results in equal improvement. The normalized plot given in Figure 6.9 more clearly shows the increased penalty of poor contact as the fin parameter is increased. For example, compare the normalized fin efficiencies for perfect contact and a/b = 0.2. From Figure 6.9, the penalty of poor contact, with $m_b = 0.1$, is only 10%; whereas with $m_b = 1.0$, the constricted contact results in a 60% loss.

Finally, consider the influence of the interstitial conductance parameter, H_{g1}, on fin efficiency for various constriction ratios and point contacts. The interstitial conductance parameter, based on convective conductance, has been defined as:

$$H_{g1} = \frac{k_{fl}\,\delta}{h\,g\,(r_t - r_b)} \tag{6.2}$$

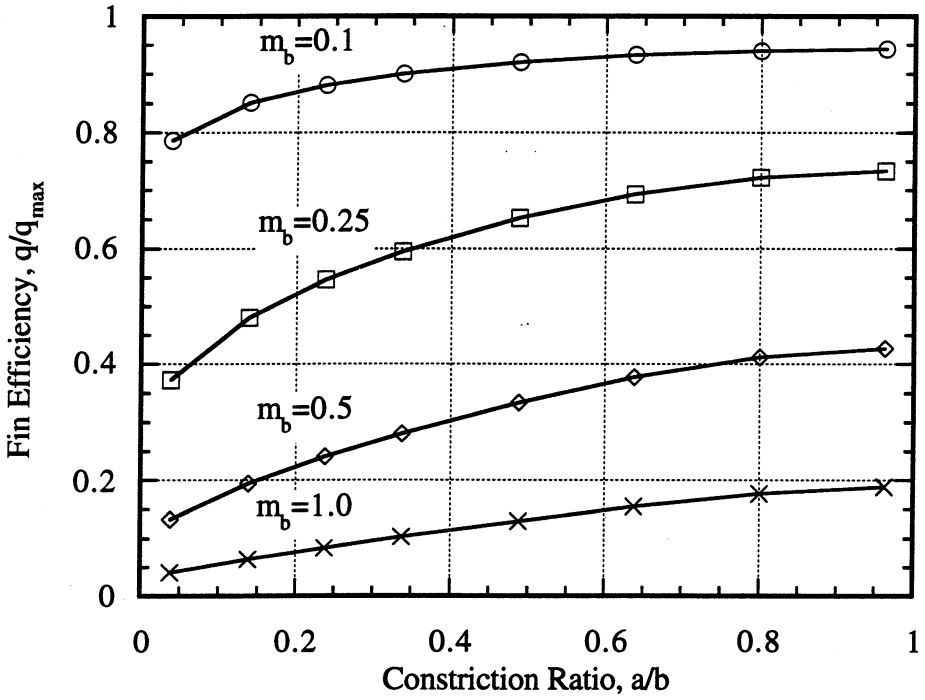

Figure 6.8. Influence of Fin Parameter on Fin Efficiency

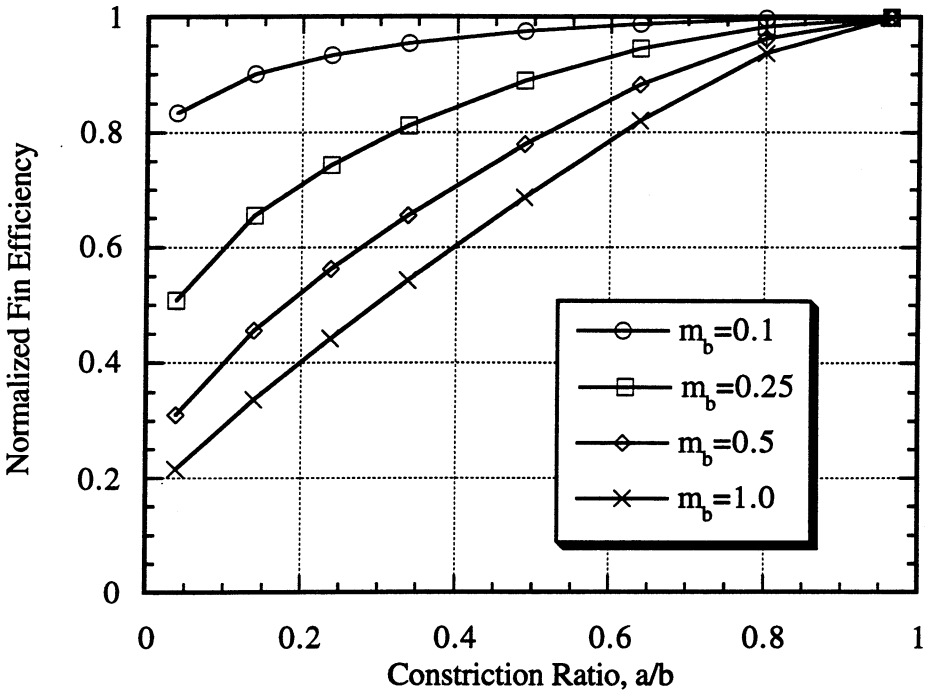

Figure 6.9. Influence of Fin Parameter on Normalized Fin Efficiency

If the fin parameter and the tip/base radius ratio are fixed, the interstitial conductance parameter basically becomes a function of the thermal conductivity of the interstitial fluid, k_{fl}, and the gap thickness, g. Using $m_b = 0.25$ and $r_t/r_b = 4$, the defined baseline case, and varying k_{fl} from 0.024 to 0.56 W/m-K and g from 0.00254 mm (0.0001 in) to 0.0508 mm (0.002 in), variable ranges established in Chapter 4, an interstitial conductance parameter range of 0.07 to 32.7 results (see Equation 6.2). Figure 6.10 illustrates the influence of this interstitial conductance parameter range on fin efficiency for constriction ratios of 0.1, 0.25 and 0.5 with one point contact. From this graph, decreasing the interstitial conductance results in a greater decline in fin efficiency at lower constriction ratios. Figure 6.11 shows a similar trend in the normalized fin efficiency.

Figure 6.11 also provides a means for justifying either an adiabatic, conductive interstitial or perfect contact boundary condition at the non-contact, fin/tube interface. Assuming that fin efficiencies within 5% of the adiabatic or perfect contact efficiencies may be considered as having those boundary conditions, a range of interstitial conductances may be established to suggest boundary condition treatment. Table 6.2 summarizes these limits for the baseline case, three constriction ratios (0.1, 0.25 and 0.5) and one point contact. Interstitial conductance values in-between these limits suggest a conductive interstitial boundary condition. As indicated from

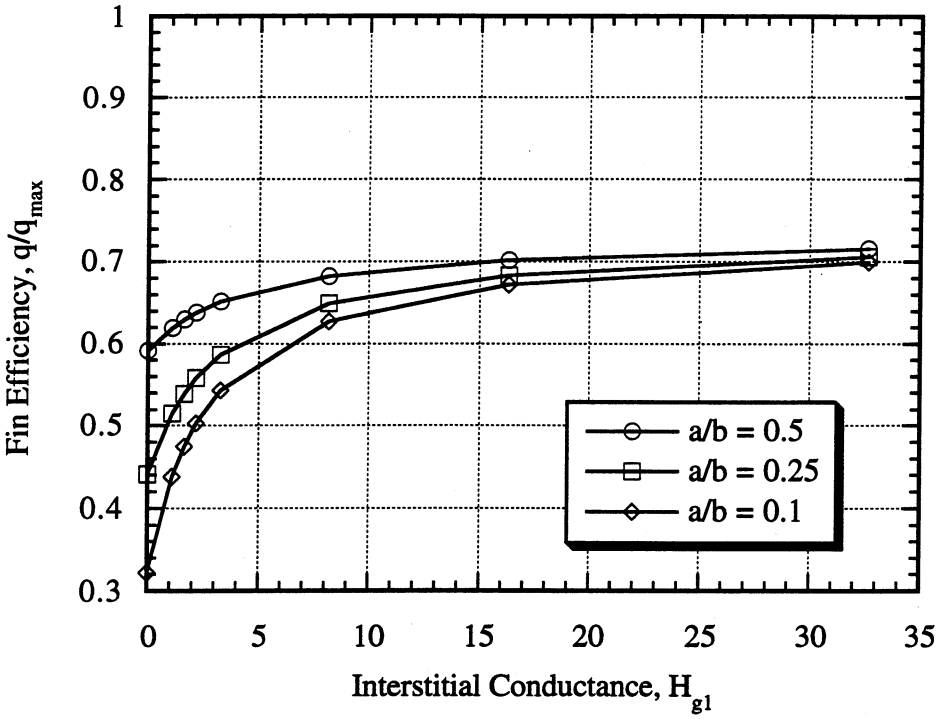

Figure 6.10. Influence of Interstitial Conductance Parameter on Fin Efficiency (One Point Contact)

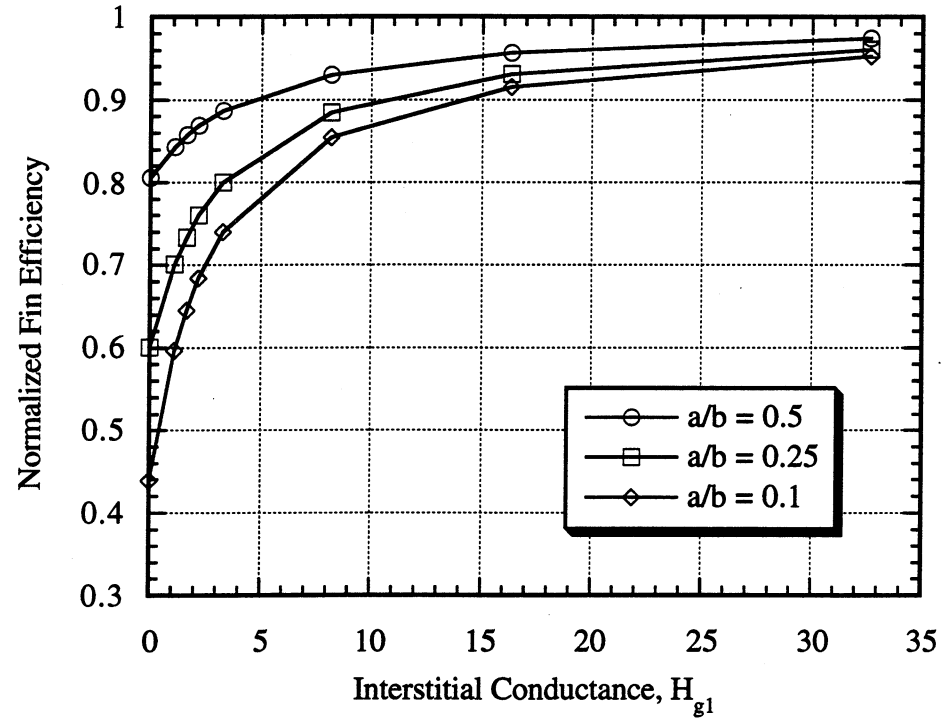

Figure 6.11. Influence of Interstitial Conductance Parameter on Normalized Fin Efficiency (One Point Contact)

Table 6.2, lower constriction ratios have a greater range where a conductive interstitial boundary condition would be appropriate.

Constriction Ratio	Interstitial Conductance, H_{g1}	
	Adiabatic Boundary	Perfect Contact Boundary
0.10	0.47	23.7
0.25	0.74	17.0
0.50	2.46	8.88

Table 6.2. Interstitial Conductance Limits Within 5% Accuracy of Adiabatic or Perfect Contact Fin Efficiency, One Point Contact

Figure 6.12 illustrates the influence of the interstitial conductance parameter on fin efficiency for two point contact (the analogous one point contact results were given in Figure 6.10). Figure 6.13 shows a similar relation for the normalized fin efficiency, and Table 6.3 presents the range of interstitial conductances which qualify boundary condition consideration for the baseline, two point contact case. Note that with a constriction ratio of 0.5, a conductive interstitial boundary is never necessary, and interstitial conductances above the perfect contact boundary limit or below the adiabatic boundary limit alter the fin efficiency by less than 4%.

Constriction Ratio	Interstitial Conductance, H_{g1}	
	Adiabatic Boundary	Perfect Contact Boundary
0.10	0.89	20.7
0.25	1.97	14.5
0.50	12.1 (4%)	12.2 (4%)

Table 6.3. Interstitial Conductance Limits Within 5% Accuracy of Adiabatic or Perfect Contact Fin Efficiency, Two Point Contact

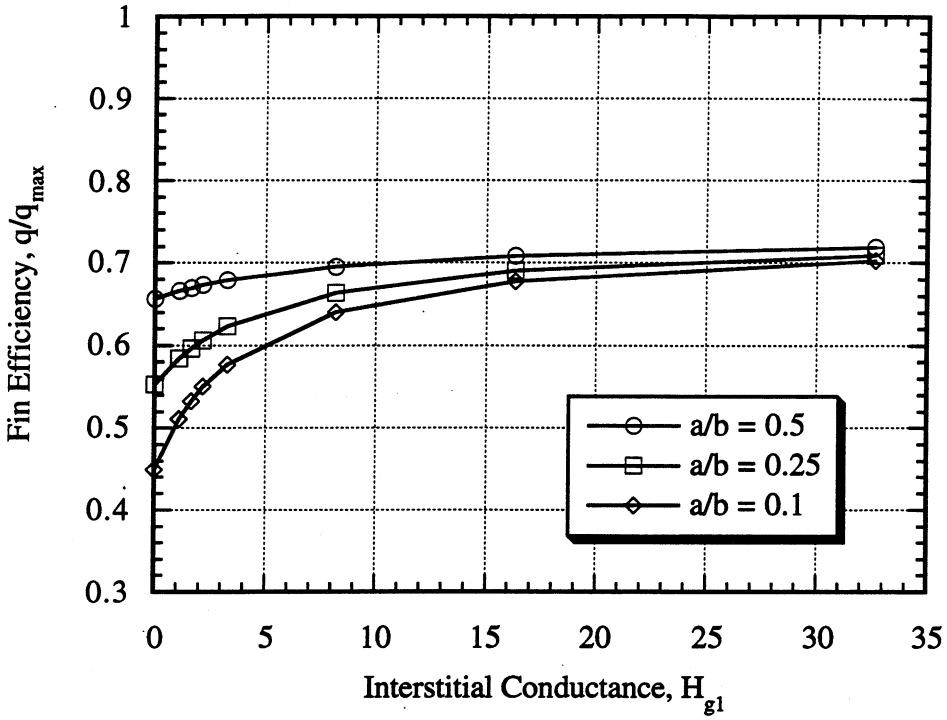

Figure 6.12. Influence of Interstitial Conductance Parameter on Fin Efficiency (Two Point Contact)

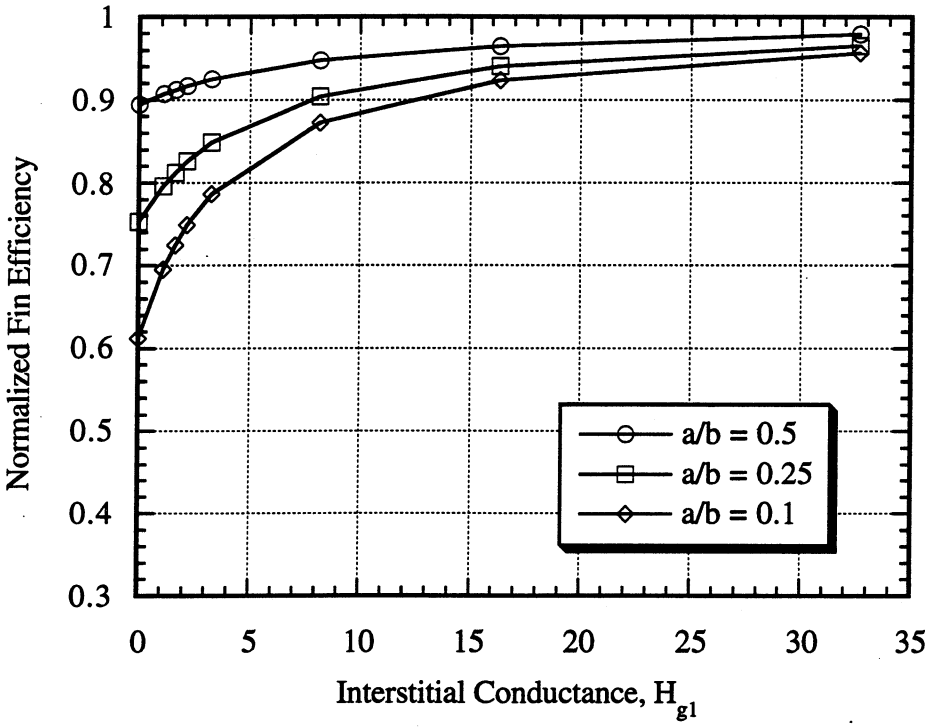

Figure 6.13. Influence of Interstitial Conductance Parameter on Normalized Fin Efficiency (Two Point Contact)

Finally, Figure 6.14 again depicts the influence of the interstitial conductance parameter on fin efficiency for the same constriction ratios and three point contact. Figure 6.15 illustrates a similar trend for the normalized fin efficiency. Once again, Table 6.4 summarizes the range of interstitial conductances which specify fitting boundary condition treatment. Note as contact points have increased, the need for a conductive interstitial boundary condition at the non-contact portion of the fin/tube interface has diminished.

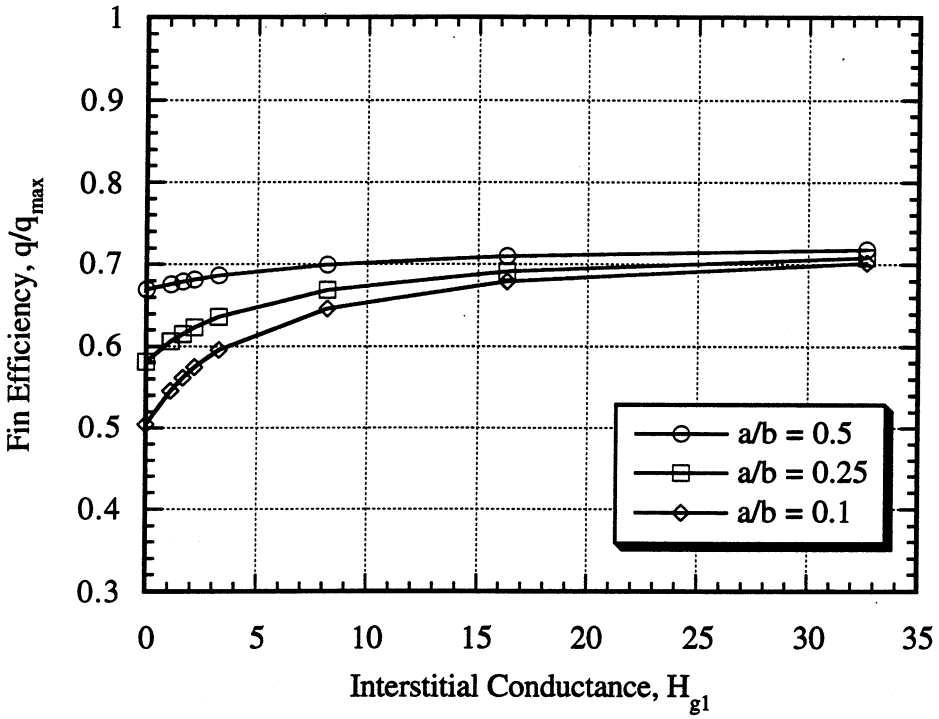

Figure 6.14. Influence of Interstitial Conductance Parameter on Fin Efficiency (Three Point Contact)

Constriction Ratio	Interstitial Conductance, H_{g1}	
	Adiabatic Boundary	Perfect Contact Boundary
0.10	1.37	20.2
0.25	2.88	13.7
0.50	10.3 (4%)	10.4 (4%)

Table 6.4. Interstitial Conductance Limits Within 5% Accuracy of Adiabatic or Perfect Contact Fin Efficiency, Three Point Contact

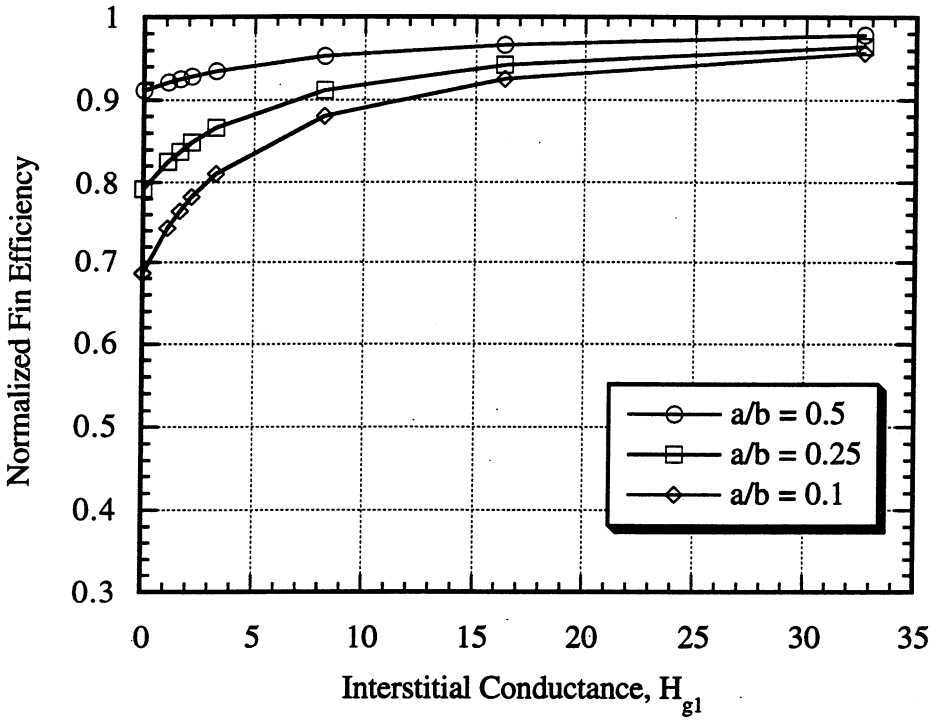

Figure 6.15. Influence of Interstitial Conductance Parameter on Normalized Fin Efficiency (Three Point Contact)

6.2 Non-Collared Plate-Fins with Frost Buildup

The influence of the fin parameter and the frost/gap thickness ratio on the fin performance of non-collared plate-fins with frost buildup is now examined. By deviating from the defined baseline case by only the fin parameter or the frost/gap thickness ratio, the magnitude of these influences will become evident. The baseline case is defined as:

$$m_e = 0.75;\ \text{Frost/Gap Thickness Ratio} = 0 \tag{6.3}$$

where m_e is the equivalent fin parameter based on the characteristic length of the fin ($r_t - r_b$), and is defined as:

$$m_e = \left(\frac{r_t}{r_b} - 1\right) m_b \tag{6.4}$$

The baseline value of the equivalent fin parameter is 0.75 (see definition of baseline case given in Equation 6.1).

Unlike the previous non-collared, plate-fin investigation, direct contact between the fin and tube is assumed absent. Hence, the only possible paths of heat flow are conduction through the interstitial substance and shunting through the frost buildup region. Because of this variation, fin efficiency or normalized fin efficiency is only a function of the fin parameter, frost/gap thickness ratio and the interstitial conductance. We define the interstitial conductance for the straight fin of rectangular profile, used in this investigation, as:

$$H_{g2} = \frac{\delta k_{fl}}{g h L_f} \tag{6.5}$$

where H_{g2} represents the ratio of the conductance across the gap to the convective conductance of the fin, defined in Chapter 4.

For the frost free baseline case, the influence of various fin parameters, 0.35, 0.5, 0.75 and 1.25, on the fin efficiency over a range of interstitial conductances is illustrated in Figure 6.16. Similarly, the influence of these same fin parameters to the normalized fin efficiency, over the same range of interstitial conductances, is shown in Figure 6.17. Note that the fin efficiencies were normalized by the perfect contact fin efficiency calculated from the equation:

$$\eta_{max} = \frac{\tanh(m_e)}{m_e} \tag{6.6}$$

The dramatic effect of the fin parameter is clearly evident in these graphs. Not only does a high fin parameter result in poorer performance, but also a greater vulnerability to low interstitial conductances. Figure 6.17 illustrates this point; fin performance begins to decrease more rapidly for high fin parameters at interstitial conductances less than 10.

Figure 6.18 illustrates the shunting of heat flow through frost buildup at the fin/tube interface for three interstitial conduction values, 1.0, 2.0 and 4.0. These interstitial conductance values are not arbitrary. Setting the fin parameter at its baseline value, 0.75, the interstitial conductance basically becomes a function of the gap thickness and the thermal conductivity of the interstitial conductance. Setting the gap thickness to a mid-range value of 0.0254 mm (0.001 in), a H_{g2} of approximately 1.0 is prescribed by a gap conductivity of frost; while, a H_{g2} of about 4.0 results from a gap conductivity of water.

Figure 6.18 shows: (i) the benefit of heat flow through the frost buildup is larger with lower gap conductivities, i.e. lower H_{g2}; and (ii) the advantage of frost buildup reaches its asymptotic value

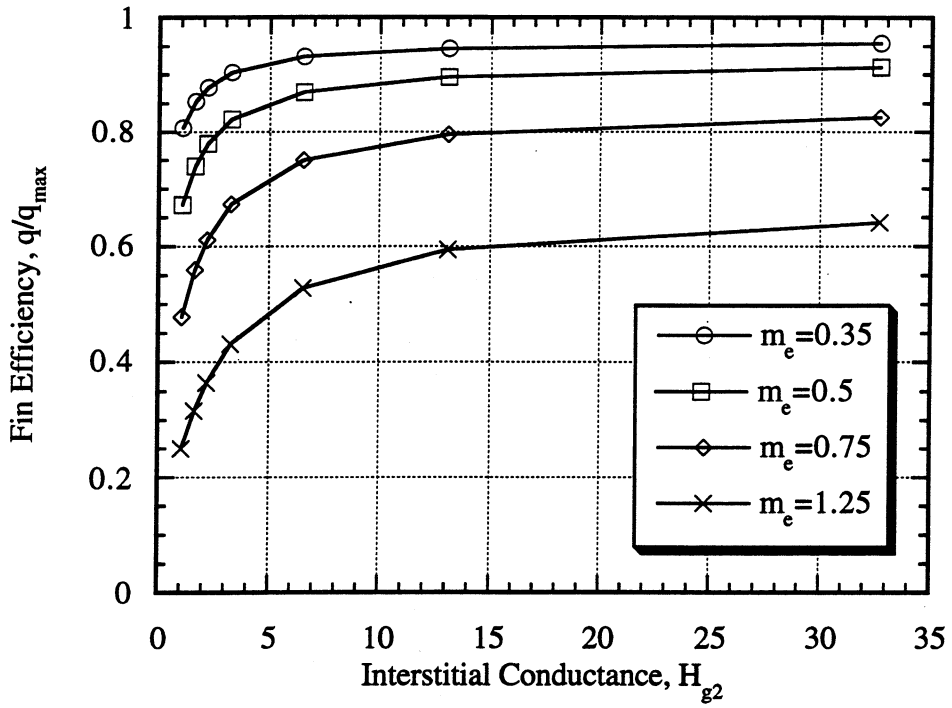

Figure 6.16. Influence of the Fin Parameter on Fin Efficiency Over a Range of Interstitial Conductances

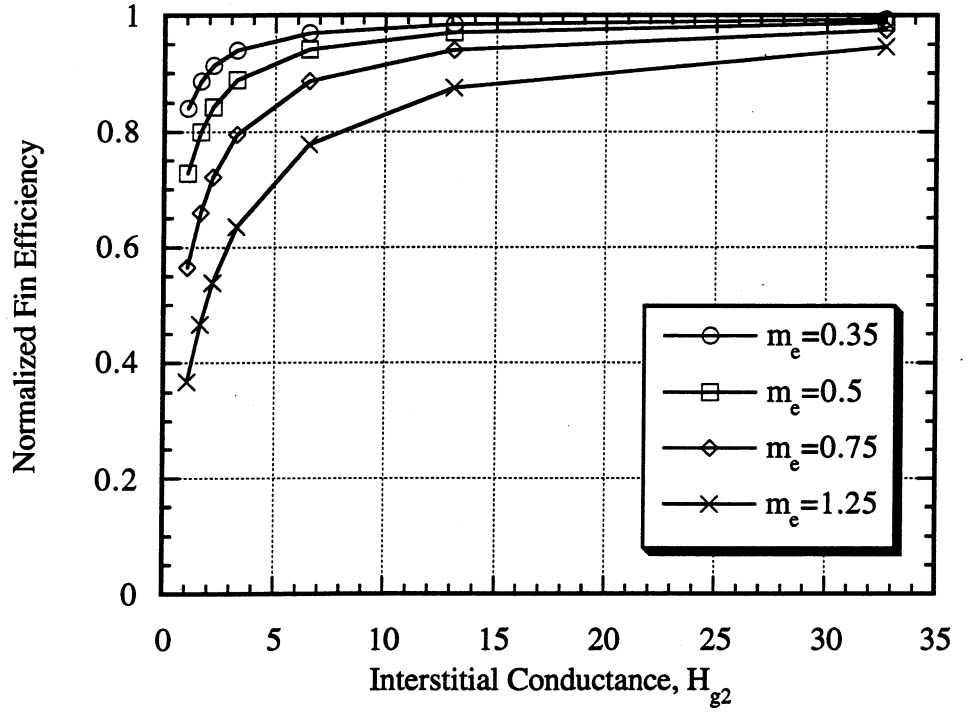

Figure 6.17. Influence of the Fin Parameter on Normalized Fin Efficiency Over a Range of Interstitial Conductances

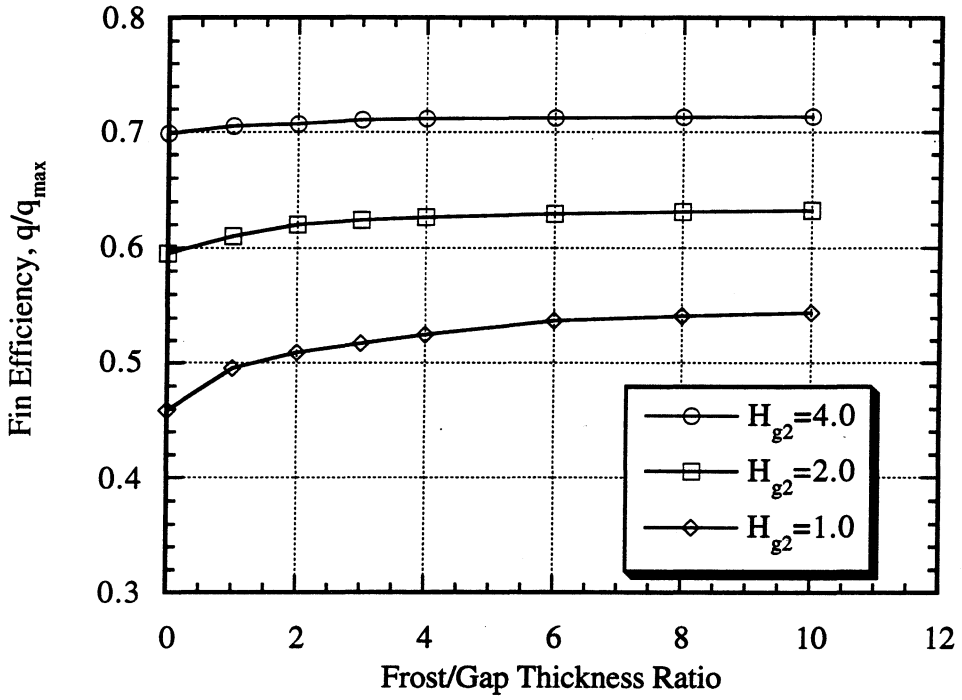

Figure 6.18. Influence of Frost Buildup on Fin Efficiency for Various Interstitial Conductances

at a frost/gap thickness ratio of approximately 8. Observing Figure 6.18, with H_{g2} = 1.0, a 9% increase in fin performance is evident at a frost/gap thickness ratio of 8; only a 1% gain is possible for H_{g2} = 4.0. Thus, frost buildup is only advantageous for low interstitial conductances.

Figure 6.19 illustrates the effect of frost buildup on fin efficiency for a range of interstitial conductances. Again, the baseline fin parameter is used, and only the thermal conductivity of the interstitial substance is varied. Note that for this particular case, a fin/gap thickness ratio of 25 represents a frost buildup of less than 5% of the fin's height. Figure 6.19 simply gives the results of Figure 6.18 plotted in a different manner. Improvement in fin efficiency drops off quickly with frost/gap thickness ratios greater than 5 and has a negligible influence with interstitial conductances greater than 7. However, the advantage to fin efficiency is considerable if air or frost were entrapped in the interstice. The interstitial conductance would be approximately 0.5 and increases in fin efficiency of 13 and 18% are possible with frost/gap thickness ratios of 5 and 25, respectfully.

Figure 6.20 shows the effect of frost buildup on normalized fin efficiency over a larger range of

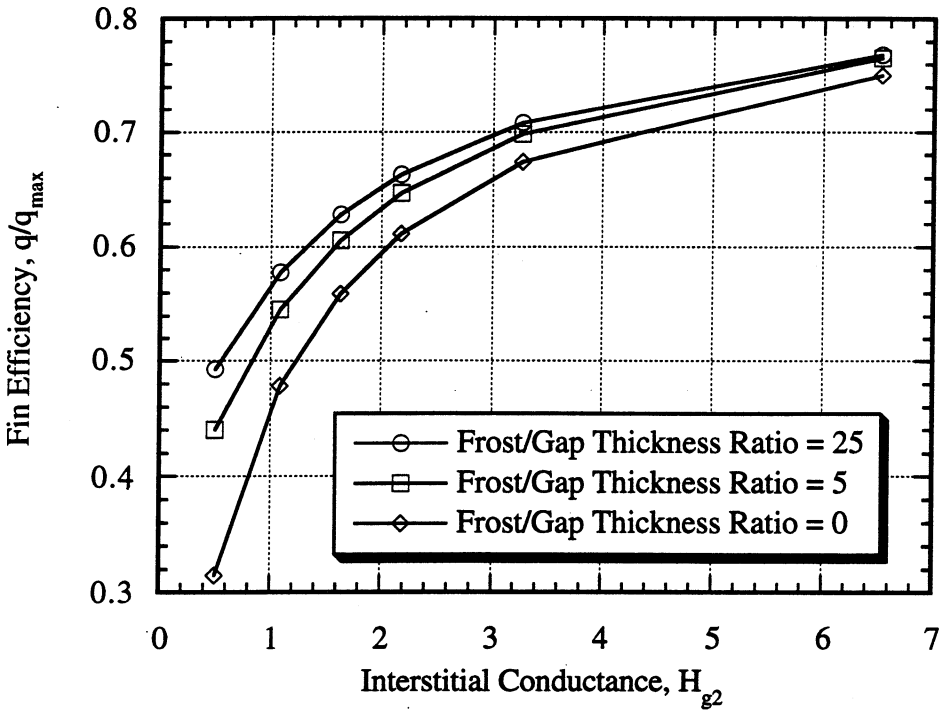

Figure 6.19. Influence of Frost Buildup on Fin Efficiency Over a Range of Interstitial Conductances

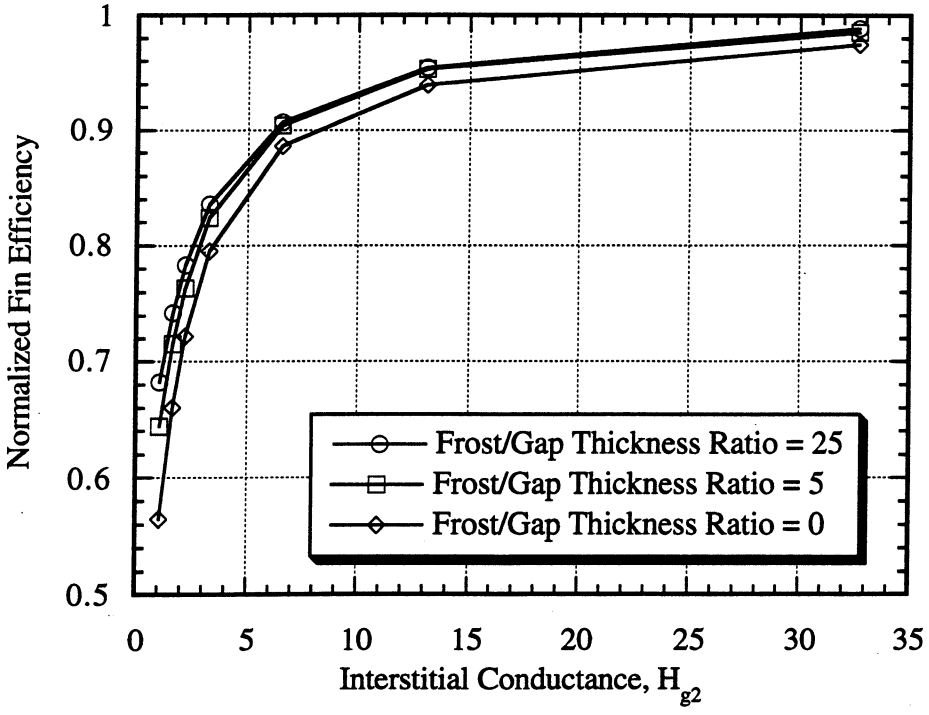

Figure 6.20. Influence of Frost Buildup on Normalized Fin Efficiency Over a Range of Interstitial Conductances

interstitial conductances. The results are consistent with the previous findings. The benefit of greater frost/gap thickness ratios ceases at interstitial conductance values of approximately 7 (as in Figure 6.19). Negligible improvements to heat flow exist when $H_{g2} > 5$; while, moderate increases in fin performance exist when $H_{g2} < 1$.

6.3. Collared Plate-Fins

The influence of tip/base radius ratio, fin parameter, fin spacing and interstitial conductance parameter on fin performance of collared plate-fins is examined in this section. By varying the above parameters individually from the baseline case, the magnitude of their influence on fin performance will be apparent. The baseline case for the collared plate-fin geometry is defined as:

$$m_b = 0.25;\ \frac{r_t}{r_b} = 4;\ 551 \text{ fins/meter (14 fins/inch)};$$
$$H_{g1} = 0 \text{ (adiabatic non-contact interface)} \tag{6.7}$$

One point contact is also defined for the reference case. Once again, the fin parameter and tip/base radius ratio are based on a typical plate-fin evaporator supplied by Peerless of America, Inc.; while, the fin spacing is based on standard, collared plate-fin construction.

Figure 6.21 illustrates the effect of various tip/base radius ratios on the baseline case over all constriction ratios. The effect of the tip/base radius ratio on fin efficiency for the collared plate-fin geometry is practically indistinguishable from the effect on the non-collared plate-fin geometry. Extending the conductive path of the fin greatly hinders fin performance, especially at high r_t/r_b ratios and lower constriction ratios.

The dependence of fin efficiency on the fin parameter, for the baseline case over all constriction ratios, is depicted in Figure 6.22. Once again, the influence of the fin parameter on fin efficiency of the collared plate-fin geometry is almost identical to the fin parameter influence of the non-collared plate-fin geometry. As the fin parameter increases, the penalty of poor macroscopic contact on fin efficiency also increases.

Next, the effect of various fin spacings (236, 551 and 787 fins/meter or 6, 14 and 20 fins/inch) on fin performance is analyzed for the baseline case. Formed collars on fins provide two functions for the collared heat exchanger: (i) they create a greater contact area with the tube to enhance conduction; and (ii) they provide a means of uniformly spacing the fins. Thus, fin spacing

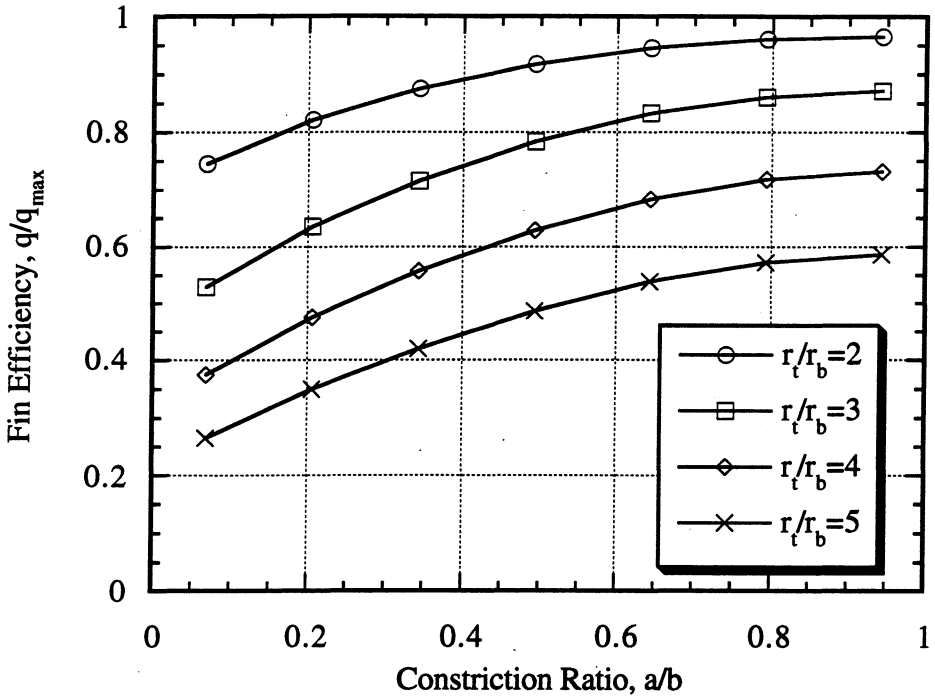

Figure 6.21. Influence of Tip/Base Radius Ratio on Fin Efficiency

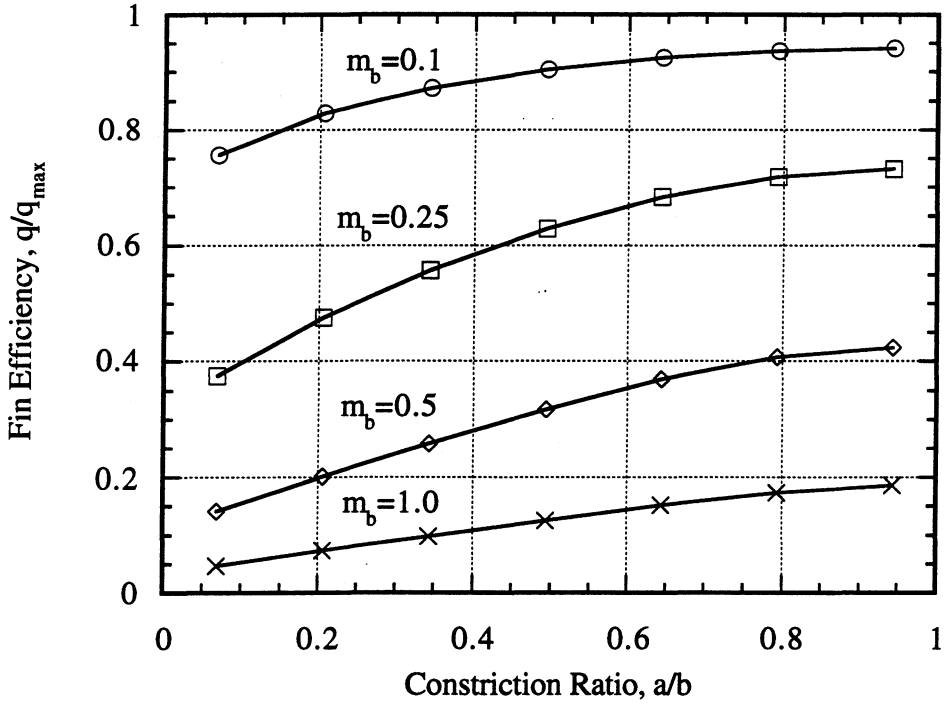

Figure 6.22. Influence of Fin Parameter of Fin Efficiency

determines the collar length. The longer the collar (the sparser the fin spacing), the greater the heat transfer (from a specific fin) and the better the fin performance. Figures 6.23 and 6.24 illustrate this trend on fin efficiency and normalized fin efficiency respectfully.

As expected, longer collars tend to alleviate the effects of decreased constriction ratios. From Figure 6.23, all fin spacings perform equally well near perfect contact (same fin efficiency of non-collared plate-fins with perfect contact). The only two factors in selecting a particular fin spacing with perfect contact, outside of frost considerations, are cost of material and the amount of heat transfer desired. However, as the constriction ratio decreases, due to poor macroscopic contact, the advantage of a larger collar to heat transfer must be investigated. From Figure 6.24, with constriction ratios around 0.25, a sparser fin spacing of 236 fins/meter would increase fin performance by 7 to 10%. Although the problem comes back to heat exchanger optimization, the advantage of a longer collar to heat flow is established.

Finally, the influence of the interstitial conductance parameter, H_{g1}, on fin performance for various constriction ratios is now presented. The interstitial conductance parameter for the collared, plate-fin geometry is identical to the non-collared, plate-fin geometry defined in Equation (6.2). Consequently, the previously calculated range of the interstitial conductance

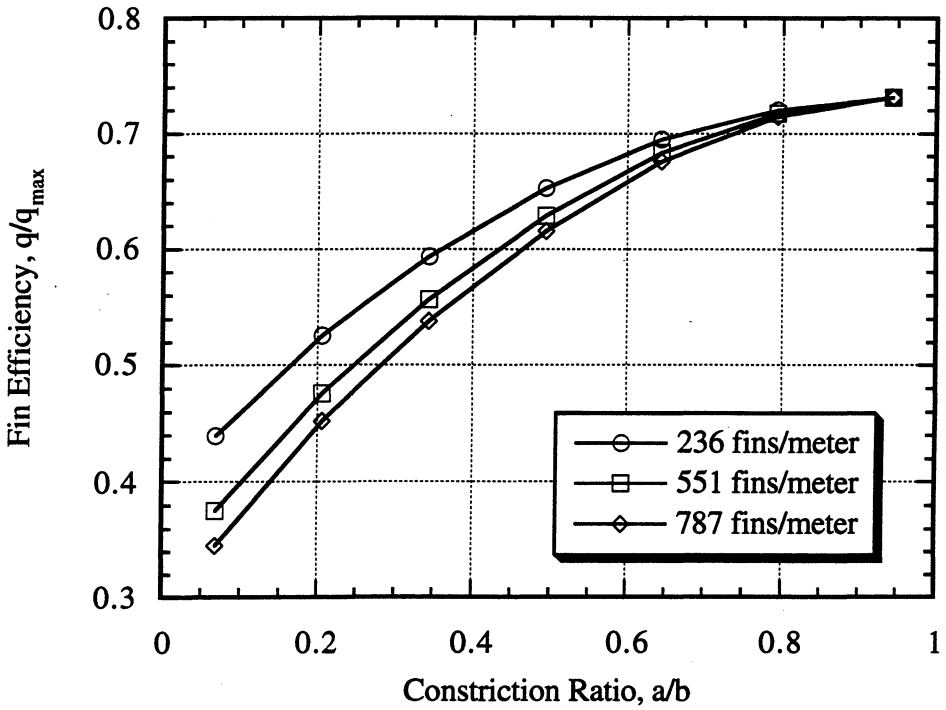

Figure 6.23. Effect of Fin Spacing on Fin Efficiency

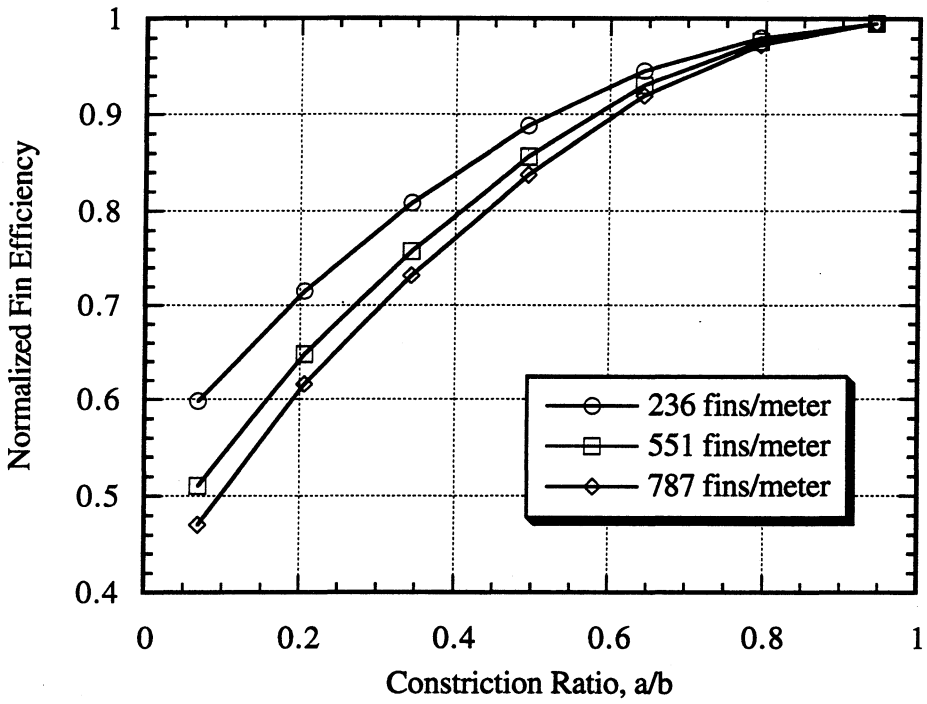

Figure 6.24. Effect of Fin Spacing on Normalized Fin Efficiency

parameter, 0.07 to 32.7, again applies to this particular geometry. Figure 6.25 shows the influence of this particular interstitial conductance parameter range on fin efficiency for constriction ratios of 0.1, 0.25 and 0.5. Figure 6.26 illustrates a similar trend for the normalized fin efficiency.

Although both of these effects are not spectacular, they establish two important points about collared plate-fins: (i) fin efficiency is not severely effected by lower constriction ratios, and (ii) fin efficiency is only effected by interstitial conductances less than 5. Information from these graphs will be expanded upon even further in the following section comparing non-collared and collared plate-fin geometries.

In addition to plotting fin efficiency against interstitial conductance for various constriction ratios, it is also of interest to vary the fin spacing. Figures 6.27, 6.28 and 6.29 illustrate the influence of the interstitial conductance on fin efficiency for various fin spacings and specific constriction ratios. Note that perfect contact asymptotes ($q/q_{max} = 0.7345$, see Table 6.1) are included on these three figures. Only at low interstitial conductances does fin spacing become a factor in fin performance. Observing Figure 6.27, all three fin spacing performance curves have

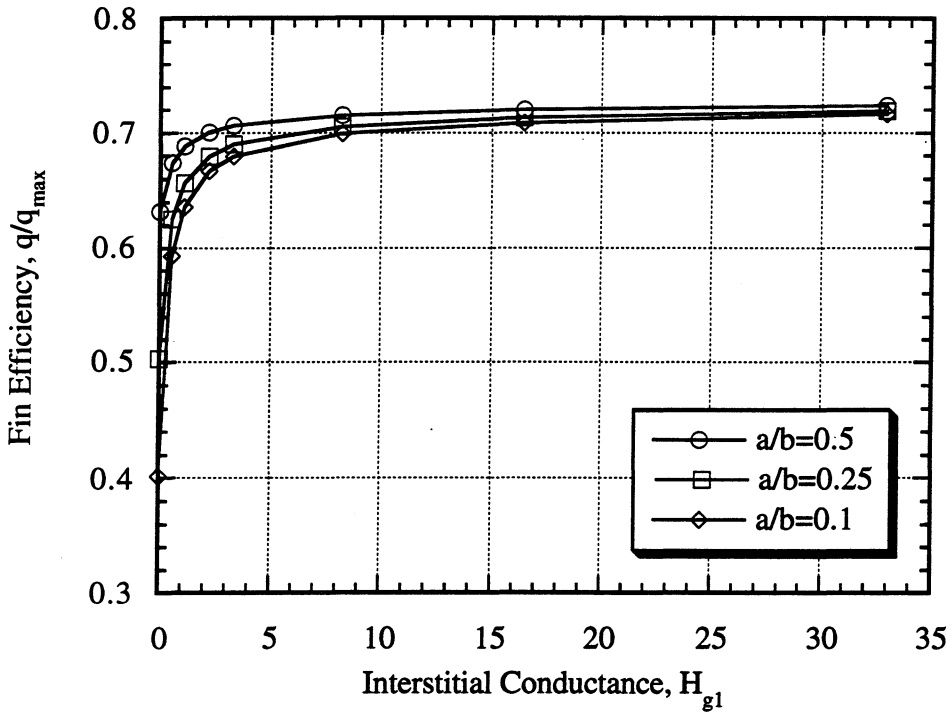

Figure 6.25. Influence of Interstitial Conductance on Fin Efficiency for Various Constriction Ratios

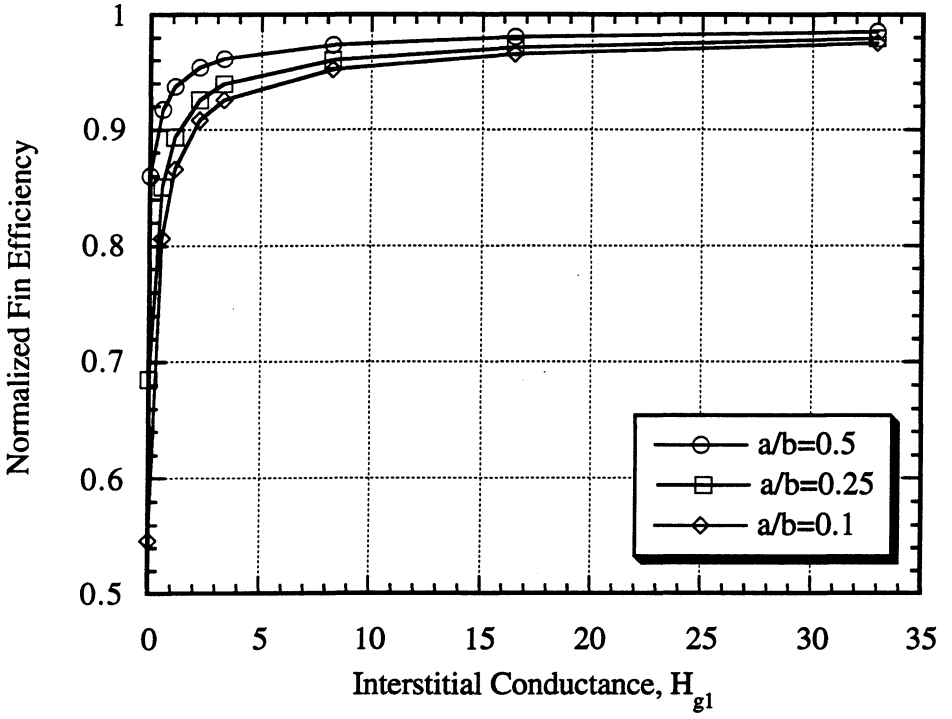

Figure 6.26. Influence of Interstitial Conductance on Normalized Fin Efficiency for Various Constriction Ratios

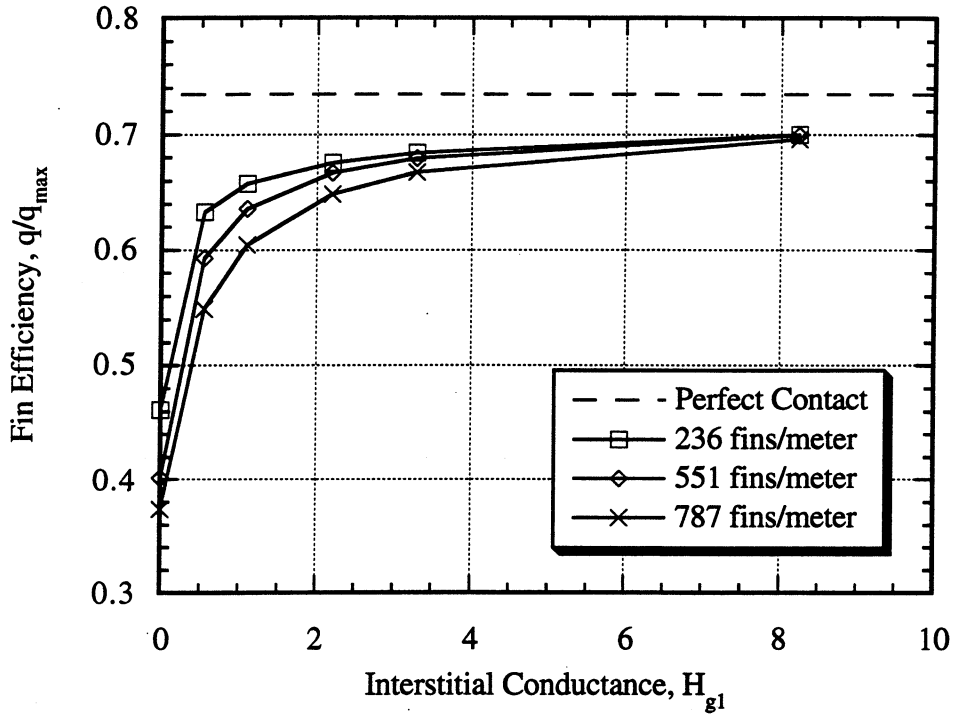

Figure 6.27. Influence of Interstitial Conductance on Fin Efficiency for Various Fin Spacings (a/b = 0.1)

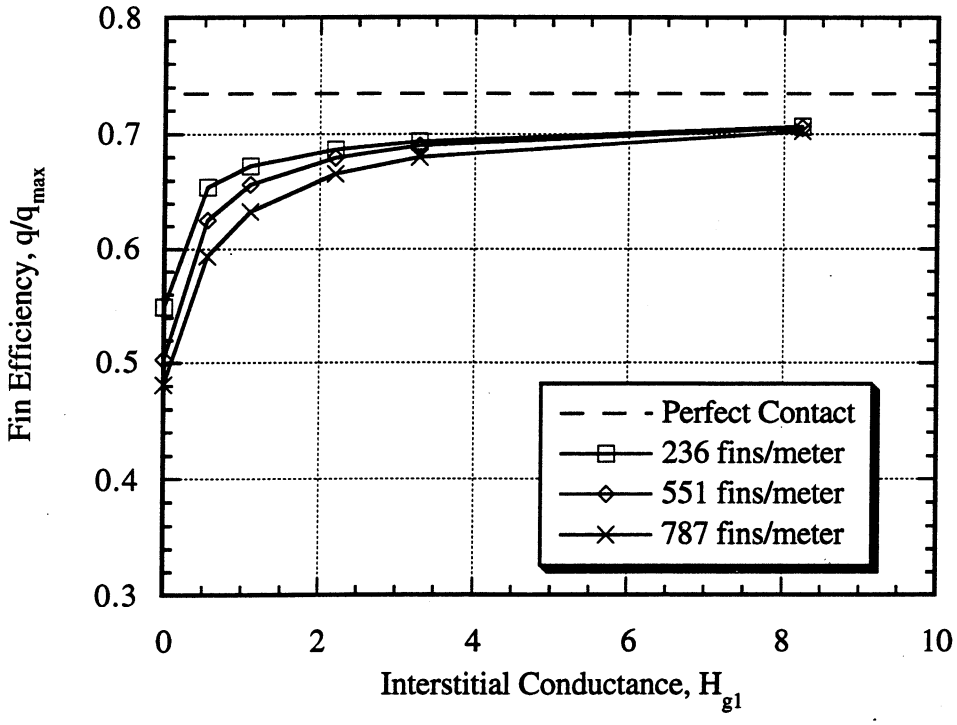

Figure 6.28. Influence of Interstitial Conductance on Fin Efficiency for Various Fin Spacings (a/b = 0.25)

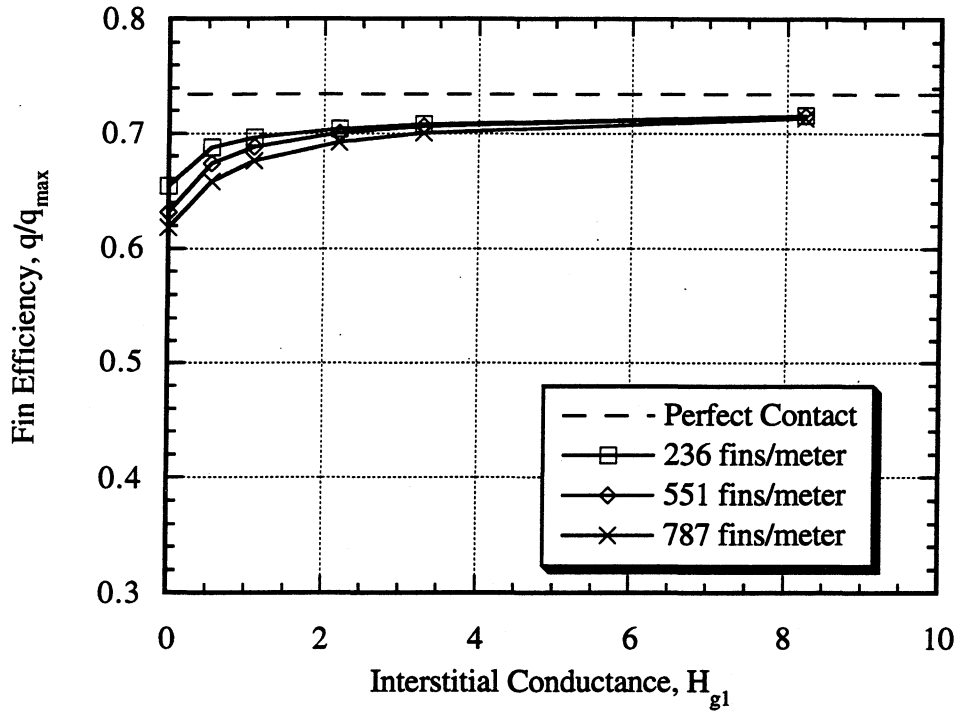

Figure 6.29. Influence of Interstitial Conductance on Fin Efficiency for Various Fin Spacings (a/b = 0.5)

fin efficiencies within 2% at $H_{g1} = 4$. From figures 6.28 and 6.29, the curves are within 2% at $H_{g1} = 3$ and 2, respectfully. Finally, it is of interest to briefly compare figures 6.27, 6.28 and 6.29 with Figure 6.23, the effect of fin spacing on fin efficiency with $H_{g1} = 0$. From Figure 6.23, as fin density decreases the advantage of the greater conductive area due to the collar becomes more pronounce, i.e. the fin spacing performance curve of 551 fins/meter approached the 787 fin/meter curve first. However, when the conductivity of the interstitial substance is taken into account (figures 6.27, 6.28 and 6.29), the decreasing of fin density resulted in a decreasing advantage of the increased collar length, i.e. the fin spacing performance curve of 551 fins/meter approached the 236 fins/meter curve first. This is due to the introduction of the interstitial substance conductivity; it damps out the disadvantage of the shorter collar.

6.4 Non-Collared and Collared Plate-Fin Comparison

In conclusion of this Numerical Results and Analysis chapter, specific distinctions between the non-collared and collared, plate-fin geometries shall be made. Intuitively, one would expect a collared plate-fin to always be superior over a non-collared one (in terms of heat transfer);

however, operating under certain constriction ratios and/or interstitial conductances, their performance is quite similar. Once again, the baseline case for both the non-collared and collared plate-fin geometries has been defined as:

$$m_b = 0.25;\ \frac{r_t}{r_b} = 4;\ H_{gl} = 0;\ 551 \text{ fins/meter (collared geometry)} \qquad (6.8)$$

During this comparison, one point contact has been used for the non-collared geometry; which is defined as baseline for the collared plate-fin.

We begin with plotting these two baseline cases over the range of constriction ratios, see Figure 6.30. Note that since the objective of this section is to compare the non-collared and collared fin geometries, normalized fin efficiency graphs are not included due to the little additional information they would provide. Also note that perfect contact asymptotes ($q/q_{max} = 0.7345$, see Table 6.1) are included on all figures within this section.

From Figure 6.30, the advantage of a collared plate-fin increases as the constriction ratio decreases. For constriction ratios greater than 0.5, less than a 5% increase in fin efficiency

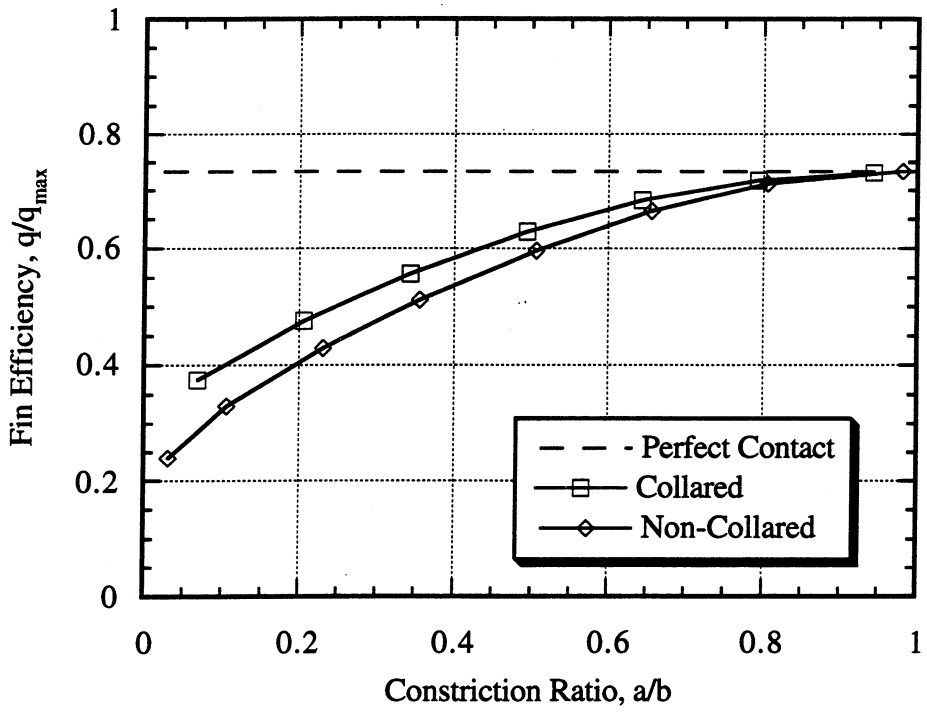

Figure 6.30. Baseline Comparison of Non-Collared and Collared Plate-Fin Geometries

occurs with the collar addition. Whereas at a constriction ratio of 0.1, an increase of only 10% is seen.

The influence of interstitial conductance on fin efficiency for non-collared and collared fin geometries is compared in figures 6.31, 6.32 and 6.33. The fin performance variations of each geometry for constriction ratios of 0.1, 0.25 and 0.5, respectfully, are presented.

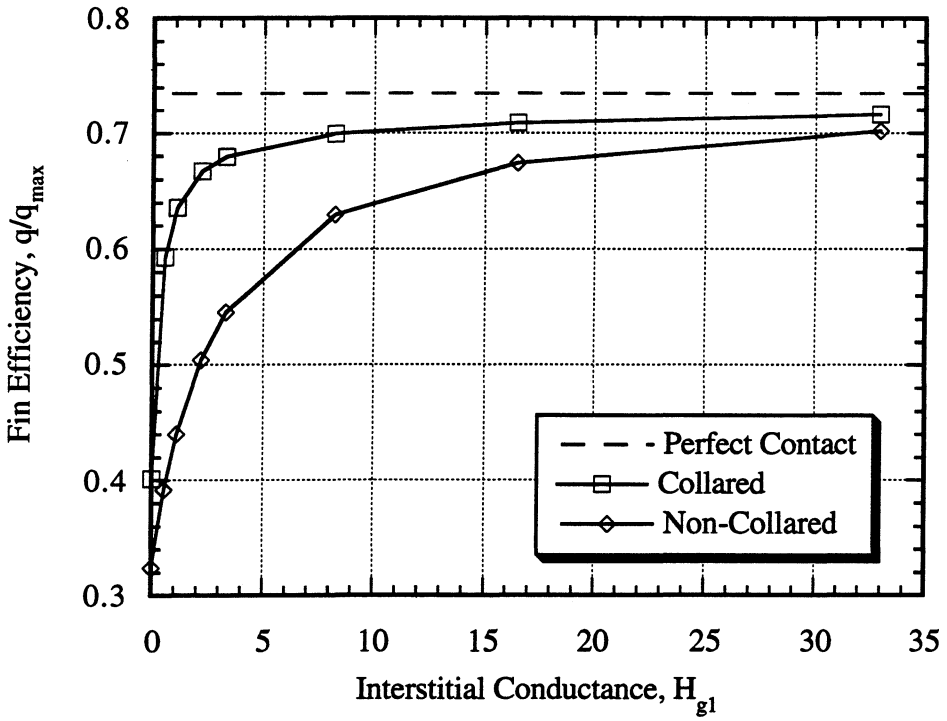

Figure 6.31. Influence of Interstitial Conductance on Fin Efficiency for Non-Collared and Collared Plate-Fins (a/b = 0.1)

When considering the conductivity of the interstitial substance, a greater advantage of the collared plate-fin is evident. Observing Figure 6.31, fin efficiency gains of greater than 5% are possible when $H_{g1} < 20$, peaking at 20% for $H_{g1} \cong 2$. Similarly, from Figure 6.32, considerable fin performance gains are made for $H_{g1} < 15$ with a peak of 15% at $H_{g1} \cong 1$. Finally, with a/b = 0.5 (Figure 6.33), fin efficiency improvements of over 5% are plausible for $H_{g1} < 10$ with a maximum of 6% at $H_{g1} \cong 1$.

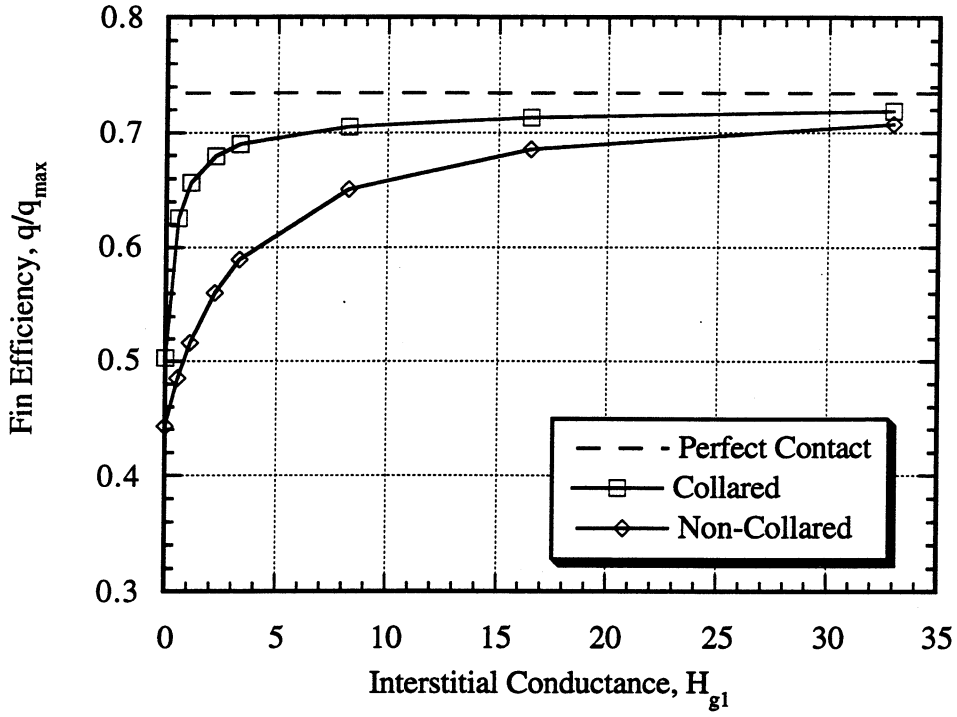

Figure 6.32. Influence of Interstitial Conductance on Fin Efficiency for Non-Collared and Collared Plate-Fins (a/b = 0.25)

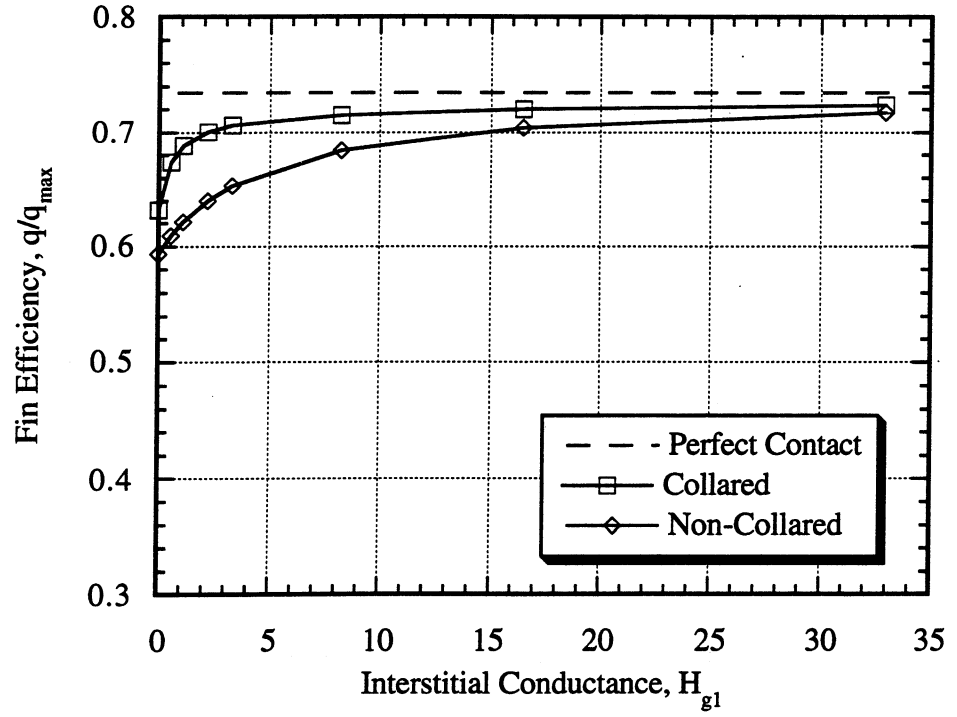

Figure 6.33. Influence of Interstitial Conductance on Fin Efficiency for Non-Collared and Collared Plate-Fins (a/b = 0.5)

Finally, Figure 6.34 combines the non-collared performance curve of Figure 6.33 with the collared performance curve of Figure 6.31. This figure shows that a poorly constructed collared plate-fin can still out-perform a better made non-collared plate-fin for interstitial conductances greater than one.

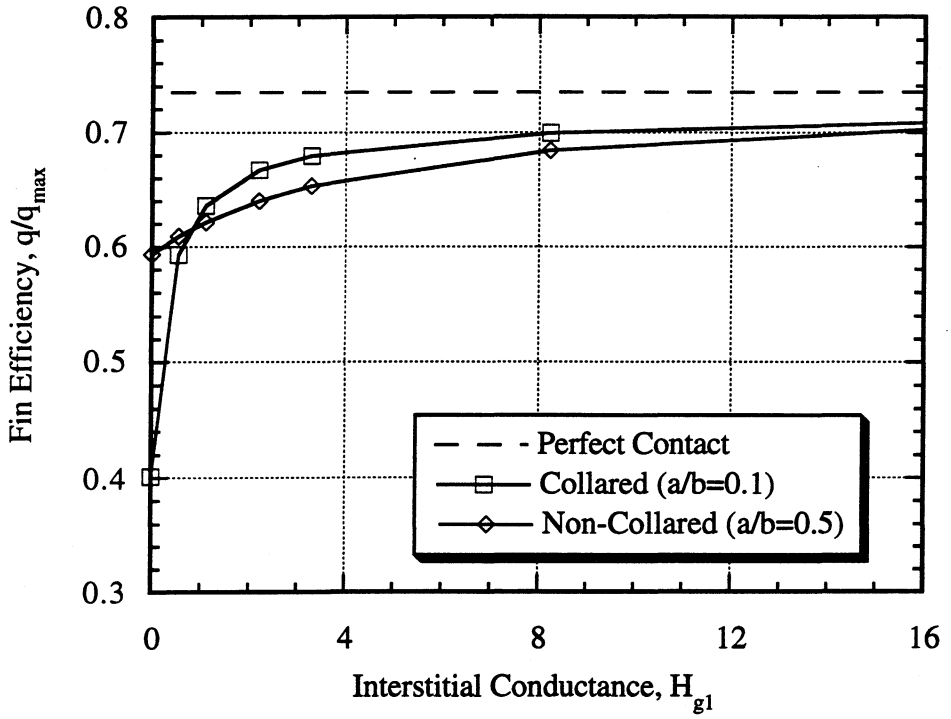

Figure 6.34. Influence of Interstitial Conductance on Fin Efficiency for Non-Collard and Collared Plate-Fins

7. CONCLUSIONS

7.1 Summary

A large amount of information was derived showing the influence of macroscopic heat flow constrictions on the performance of fin/tube heat exchangers. The following is a summary of the numerical results, categorized by the specific cases investigated:

Non-Collared Plate-Fins

1. Location of the actual contact area about the fin/tube interface is as important as the constriction ratio itself.

2. Lower tip/base radius ratios provide a more efficient fin.

3. Constriction resistance becomes more severe as the fin parameter increases.

4. The interstitial conductance parameter, H_{g1}, provides a means of determining boundary conditions at the non-contact areas of the fin/tube interface:
   a. If $H_{g1} >> 1$ then a perfect contact boundary condition can be used.
   b. If $H_{g1} << 1$ then an adiabatic boundary condition can be used.
   c. If $H_{g1} \approx 1$ then a conductive interface boundary condition must be used.

Non-Contact Plate-Fin with Frost Buildup

1. Frost buildup along the non-contact areas of the fin/tube interface can benefit fin performance when the interstitial conductance parameter, H_{g2}, is less than 2.

2. Frost thicknesses greater than 8 times the gap thickness provide no additional benefit to fin performance for all values of H_{g2}.

Collared Plate-Fins

1. The influence of the tip/base radius ratio and the fin parameter to fin performance is similar to the non-collared plate-fins.

2. Lower fin spacings, i.e. increase collar area, improves fin performance of an individual fin; however the overall heat transfer is reduced because of the reduction in the total number of fins.

3. At lower fin spacings, the interstitial conductance parameter, H_{g1}, has a greater influence on fin efficiency as the constriction ratio decreases.

4. Fin efficiency is not severely effected at lower constriction ratios when $H_{g1} > 5$.

5. Collared plate-fins improve fin efficiency by at least 10% over non-collared plate-fins for constriction ratios less than 0.5.

7.2 Recommendations

Experimental verification of all results within this investigation is recommended before directly applying to any fin/tube heat exchanger designs. When designing an experimental program, one will find the following three variables difficult to establish: (i) the constriction ratio, (ii) the heat transfer coefficient and (iii) the gap thickness. The following suggestions are made by the author in order to determine these variables. This discussion is by no means complete.

One method to estimate the constriction ratio would be to measure the imprint left on the tube by the fin after removal. This distance could then be divided by the outside circumference of the tube. The heat transfer coefficient could be estimated by two methods: (i) one could use the papers by Shepard (1956) and Rich (1975), as did this investigation or (ii) determine the coefficient experimentally by using an identical fin/tube heat exchanger with a constriction resistance of zero, i.e. a fin/tube interface metallurgically bonded. At this time, a reasonable method in measuring the gap thickness has not been resolved. Determining the magnitude of the gap, which would not be difficult, may be adequate in establishing an interstitial conductance range for investigation.

REFERENCES

ASHRAE, 1989, *ASHRAE Handbook - 1989 Fundamentals*, Atlanta: American Society of Heating, Refrigerating and Air-Conditioning Engineers, Chapter 3, pp. 19-20.

Christensen, R. N., and Fernandes, H. V., 1983, "Contact and Fouling Resistances in Finned Tube Heat Exchangers," ASME Paper No. 83-HT-39.

Clausing, A. M., 1963, "Thermal Contact Resistance in a Vacuum Environment," Ph. D. Thesis, University of Illinois, Urbana, Illinois.

Clausing, A. M., 1965, "Some Influences of Macroscopic Constrictions on Thermal Contact Resistance," *University of Illinois Engineering Experiment Station Report*, ME-TN-242-2.

Clausing, A. M., 1988, "Numerical Methods in Heat Transfer," Lecture Notes, University of Illinois, Urbana, Illinois.

Dart, D. M., 1959, "Effect of Fin Bond on Heat Transfer," *ASHRAE J.*, Vol. 1, No. 5, pp. 67-71.

Dietenberger, M. A., 1983, "Generalized Correlation of the Water Frost Thermal Conductivity," *Int. J. of Heat and Mass Transfer*, Vol. 26, No. 4, pp. 607-619.

Eckels, P. W., 1977, "Contact Conductance of Mechanically Expanded Plate Finned Tube Heat Exchangers," ASME Paper No. 77-HT-24.

Ernest, T. L., Sheffield, J. W., and Sauer, H. J., 1985, "Finned Tube Contact Conductance: Characterizing the Integrity of the Mechanical Bond," *ASHRAE Trans.*, Vol. 91, Pt. 2A, pp. 85-99.

Fletcher, L. S., 1988, "Recent Developments in Contact Conductance Heat Transfer," *J. of Heat Transfer*, Vol. 110, pp. 1059-1070.

Gardner, K. A., and Carnavos, T. C., 1960, "Thermal-Contact Resistance in Finned Tubing," *J. of Heat Transfer*, Vol. 82, No. 2, pp. 279-293.

Gates, R. R., Sepsy, C. F. and Huffman, G. D., 1967, "Heat Transfer and Pressure Loss in Extended Surface Heat Exchangers Operating Under Frosting Conditions - Pt. 1," *ASHRAE Trans.*, Vol. 73, Pt. 2, pp. 2.1-2.13.

Gebhart, B., 1993, *Heat Conduction and Mass Transfer*, New York: McGraw-Hill Book Co., pp. 399-425.

Hrnjak, P. S., and Sheffield, J. W., 1990, "Contact Resistance in Plate Finned Tubes Heat Exchangers: State-of-the-Art," *Proceedings of the 9th International Heat Transfer Conference*, Jerusalem, Israel, pp. 9-14.

Huffman, G. D., and Sepsy, C. F., 1967, "Heat Transfer and Pressure Loss in Extended Surface Heat Exchangers Operating Under Frosting Conditions - Pt. 2," *ASHRAE Trans.*, Vol. 73, Pt. 2, pp. 3.1-3.16.

Incropera, F. P., and DeWitt, D. P., 1990, *Fundamentals of Heat and Mass Transfer*, Third Edition, New York: Wiley and Sons, Inc., pp. 86-88, 123.

Kays, W. M., and London, A. L., 1984, *Compact Heat Exchangers*, Third Edition, New York: McGraw-Hill Book Co., pp. 156-185.

Kern, D. Q., and Kraus, A. D., 1972, *Extended Surface Heat Transfer*, New York: McGraw-Hill Book Co., pp. 548-557.

Kondepudi, S. N., and O'Neal, D. L., 1987, "The Effects of Frost Growth on Extended Surface Heat Exchangers: A Review," *ASHRAE Trans.*, Vol. 93, Pt. 2, pp. 258-274.

Kondepudi, S. N., 1988, "The Effects of Frost Growth on Finned Tube Heat Exchangers Under Laminar Flow," Ph. D. Thesis, Texas A&M University, College Station, Texas.

Kondepudi, S. N., and O'Neal, D. L., 1993, "Performance of finned-tube heat exchangers under frosting conditions: I. Simulation model," *Int. J. of Refrigeration*, Vol. 16, No. 3, pp. 175-180.

Kondepudi, S. N., and O'Neal, D. L., 1993, "Performance of finned-tube heat exchangers under frosting conditions: II. Comparison of experimental data with model," *Int. J. of Refrigeration*, Vol. 16, No. 3, pp. 181-184.

Lemczyk, T. F., and Yovanovich, M. M., 1987, "New Models and Methodology for Predicting Thermal Contact Resistance in Compound Cylinders and Finned Tubes," *Heat Transfer Engineering*, Vol. 8, No. 2, pp. 35-48.

Madhusudana, C. V., and Fletcher, L. S., 1986, "Contact Heat Transfer--The Last Decade," *AIAA J.*, Vol. 24, No. 3, pp. 510-523.

Manzoor, M., Ingham, D. B., and Heggs, P. J., 1984, "The Accuracy of Perfect Contact Fin Analyses," *J. of Heat Transfer*, Vol. 106, No. 2, pp. 234-237.

Nho, K. M., and Yovanovich, M. M., 1989, "Measurement of Contact Resistance in Finned Tube Heat Exchangers," *ASHRAE Trans.*, Vol. 95, Pt. 1, pp. 370-377.

O'Neill, P. J., 1988, "Thermal Performance Analysis of Finned-Tube Heat Exchangers at Low Temperatures and Airflow Rates," M. S. Thesis, University of Illinois, Urbana, Illinois.

Rich, D. G., 1975, "The Effect of the Number of Tube Rows on Heat Transfer Performance of Smooth Plate Fin-and-Tube Heat Exchangers," *ASHRAE Trans.*, Vol. 81, Pt. 1, pp. 307-317.

Sauer, H. J., 1993, "Significance of Thermal Contact Resistance on Performance and Size of Finned Tube Heat Exchangers," SAE Technical Paper No. 931116.

Sauer, H. J., and Sheffield, J. W., 1985, "A Correlation for the Contact Conductance in Finned Tube Heat Exchangers," *Proceedings of the 19th International Thermal Conductivity Conference*, Cookeville, TN, pp. 289-300.

Sheffield, J. W., Abu-Ebid, M., and Sauer, H. J., 1985, "Finned Tube Contact Conductance: Empirical Correlation of Thermal Conductance," *ASHRAE Trans.*, Vol. 91, Pt. 2, pp. 100-116.

Sheffield, J. W., Sauer, H. J., and Wood, R. A., 1987, "An Experimental Method for Measuring the Thermal Contact Resistance of Plate Finned Tube Heat Exchangers," *ASHRAE Trans.*, Vol. 93, Pt. 2, pp. 776-785.

Sheffield, J. W., Stafford, B. D., and Sauer, H. J., 1985, "Finned-Tube Contact Conductance: Investigation of Contacting Surfaces," *ASHRAE Trans.*, Vol. 91, Pt. 1, pp. 442-451.

Sheffield, J. W., Wood, R. A., and Sauer, H. J., 1989, "Experimental Investigation of Thermal Conductance of Finned Tube Contacts," *Experimental Thermal and Fluid Science*, Vol. 2, No. 1, pp. 107-121.

Shepherd, D. G., 1956, "Performance of One-Row Tube Coils with Thin-Plate Fins, Low Velocity Forced Convection," *Heating, Piping & Air Conditioning*, Vol. 28, No. 4, pp. 137-144.

Stoecker, W. F., 1957, "How Frost Formation on Coils Affects Refrigeration Systems," *Refrigerating Engineering*, Vol. 65, No. 2, pp. 42-46.

Stoecker, W. F., and Jones, J. W., 1986, *Refrigeration and Air Conditioning*, New York: McGraw-Hill Book Co., pp. 239-257.

Taborek, J., 1987, "Bond Resistance and Design Temperatures for High-Finned Tubes -- A Reappraisal," *Heat Transfer Engineering*, Vol.8, No. 2, pp. 26-34.

Tio, K. K., and Sadhal, S. S., 1991, "Analysis of Thermal Constriction Resistance with Adiabatic Circular Gaps," *J. Thermophysics*, Vol. 5, No. 4, pp. 550-559.

Tio, K. K., and Sadhal, S. S., 1992, "Thermal Constriction Resistance: Effects of Boundary Conditions and Contact Geometries," *Int. J. Heat and Mass Transfer*, Vol. 35, No. 6, pp. 1533-1544.

Wilson, E. E., 1915, "A Basis for Rational Design of Heat Transfer Apparatus," *ASME Trans.*, Vol. 37, pp. 47-82.

Wood, R. A., Sheffield, J. W., and Sauer, H. J., 1987, "Thermal Contact Conductance of Finned Tubes: A Generalized Correlation," *ASHRAE Trans.*, Vol. 93, Pt. 2, 786-797.

Wood, R. A., Sheffield, J. W., and Sauer, H. J., 1987, "Thermal Contact Conductance of Finned Tubes: The Effect of Various Parameters," *ASHRAE Trans.*, Vol. 93, Pt. 2, 798-809.

Young, E. H., and Briggs, D. E., 1965, "Bond Resistance of Bimetalic Finned Tubes," *Chemical Engineering Progress*, Vol. 61, No. 7, pp. 71-79.

Yovanovich, M. M., 1986, "Recent Developments in Thermal Contact, Gap and Joint Conductance Theories and Experiment," *Proceedings of the 8th International Heat Transfer Conference*, San Francisco, CA, pp. 35-45.

APPENDIX: ANALYTICAL SOLUTION FOR 1-D CONDUCTION THROUGH AN INTERSTICE AND FIN

The problem is illustrated and the variables defined in Figure A.1. A subscript of 1 refers to the fin condition, while a subscript of 2 refers to the gap condition.

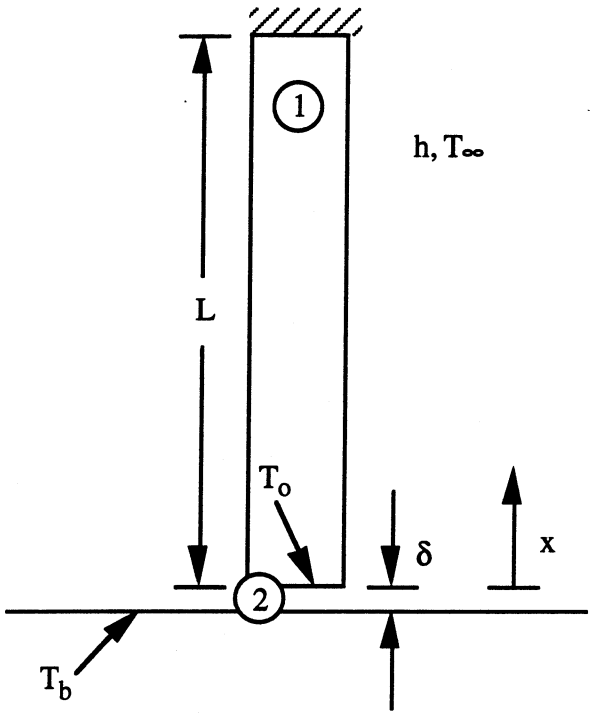

Figure A.1: Fin Geometry

The following assumptions are employed:

1. The fin is at steady state conditions.
2. Heat flow is one-dimensional in the x-direction.
3. The boundary at x = L is adiabatic.
4. The cross sectional area, A_c, is constant.
5. The heat transfer coefficient, h, and the ambient temperature, T_∞, are constants over the fin surface.
6. Conduction is the only heat transfer mode across the interstice.
7. The thermal conductivities of the fin and interstitial fluid are constants.
8. No heat generation is present.

We begin with the following form of an energy balance applied to the fin region (Incroperia and DeWitt, 1990):

$$\frac{d^2 T}{dx^2} - \frac{h P}{k_1 A_c}(T - T_\infty) = 0 \tag{A.1}$$

where P is the fin perimeter. Now let us define the heat flow across the fin base:

$$\frac{q}{A_c} = - k_1 \left.\frac{dT}{dx}\right|_{x=0} = \frac{k_2}{\delta}(T_b - T_o) \tag{A.2}$$

Next, let us define the following dimensionless variables:

$$x^* = \frac{x}{L};\ T^* = \frac{T - T_\infty}{T_b - T_\infty};\ \delta^* = \frac{\delta}{L};$$
$$m_1^2 = \frac{h P L^2}{k_1 A_c};\ m_2^2 = \frac{h P L^2}{k_2 A_c} \tag{A.3a,b,c,d,e}$$

Equation (A.1) now takes the form:

$$\frac{d^2 T^*}{dx^{*2}} - m_1^2 T^* = 0 \tag{A.4}$$

with the following boundary conditions:

$$\left.\frac{dT^*}{dx^*}\right|_{x^*=1} = 0$$
$$\left.\frac{dT^*}{dx^*}\right|_{x^*=0} = - \frac{k_2}{k_1 \delta^*}\left(1 - T_o^*\right) \tag{A.5a,b}$$

where Boundary Condition (A.5b) is Equation (A.2) nondimensionalized. The solution of Equation (A.4) takes the form:

$$T^* = C_1 \sinh(m_1 x^*) + C_2 \cosh(m_1 x^*) \tag{A.6}$$

and differentiating with respect to x^* we have:

$$\frac{d\,T^*}{dx^*} = C_1\, m_1 \cosh(m_1\, x^*) + C_2\, m_1 \sinh(m_1\, x^*) \tag{A.7}$$

From Boundary Condition (A.5a), we have:

$$0 = C_1 \cosh(m_1) + C_2 \sinh(m_1) \tag{A.8}$$

From Boundary Condition (A.5b), we have:

$$C_1 = -\frac{k_2\,(1 - T_o^*)}{k_1\,\delta^*\,m_1} \tag{A.9}$$

Plugging Equation (A.9) into (A.8) results in:

$$C_2 = -\frac{k_2\,(1 - T_o^*)\cosh(m_1)}{k_1\,\delta^*\,m_1\sinh(m_1)} \tag{A.10}$$

Substituting C_1 and C_2, Equation (A.6) becomes:

$$T^* = \frac{k_2\,(1 - T_o^*)}{k_1\,\delta^*\,m_1}\left[\frac{\cosh(m_1\,x^*)}{\tanh(m_1)} - \sinh(m_1\,x^*)\right] \tag{A.11}$$

Now, T_o^* must be defined with known quantities. Let us define:

$$\eta = \frac{q}{q_{max}} \tag{A.12}$$

where $q_{max} = P\,L\,h\,(T_b - T_\infty)$ and η is the fin efficiency. Nondimensionalizing Equation (A.2) results in:

$$\eta = \frac{1}{m_2^2\,\delta^*}\left(1 - T_o^*\right) \tag{A.13}$$

We also know:

$$q = \sqrt{k_1 A_c h P}\,(T_o - T_\infty)\tanh(m_1) \tag{A.14}$$

Nondimensionalizing (A.14) by q_{max} and setting it equal to (A.13) results in:

$$T_o^* = \frac{m_1}{m_2^2\,\delta^*\tanh(m_1) + m_1} \tag{A.15}$$

Plugging into Equation (A.11), we have the temperature distribution of the fin in the form:

$$T^* = \frac{k_2\,m_2^2\left[\cosh(m_1\,x^*) - \tanh(m_1)\sinh(m_1\,x^*)\right]}{k_1\,m_1\left[m_2^2\,\delta^*\tanh(m_1) + m_1\right]} \tag{A.16}$$

It can be shown that the fin efficiency may be defined as:

$$\eta = -\frac{1}{m_1^2}\frac{dT^*}{dx^*}\bigg|_{x^*=0} \tag{A.17}$$

Our final solution is:

$$\eta = \frac{k_2\,m_2^2\tanh(m_1)}{k_1\,m_1^2\left[m_2^2\,\delta^*\tanh(m_1) + m_1\right]} \tag{A.18}$$